Asian Journal of Electrical and Electronic Engineering

Volume 5 Issue 1 March 2025

eISSN 2785-8189

https://alambiblio.com/ojs/index.php/ajoeee

AIMS & SCOPE OF THE ASIAN JOURNAL OF ELECTRICAL AND ELECTRONIC ENGINEERING

The **Asian Journal of Electrical and Electronic Engineering** (**AJoEEE**), published biannually (March and September), is a peer-reviewed open-access journal of the **AlamBiblio Press**.

The Asian Journal of Electrical and Electronic Engineering publishes original research findings as regular papers and review papers (by invitation). The Journal provides a platform for Engineers, Researchers, Academicians, and Practitioners who are highly motivated to contribute to the Electrical and Electronics Engineering disciplines. It also welcomes contributions that address the developing world's specific challenges and address science and technology issues from a multidisciplinary perspective.

REFEREES' NETWORK

All papers submitted to AJoEEE Journal will be subjected to a rigorous reviewing process through a worldwide network of specialized and competent referees. Each accepted paper should have at least two positive referees' assessments.

SUBMISSION OF A MANUSCRIPT

A manuscript should be submitted online to the Asian Journal of Electrical and Electronic Engineering (AJoEEE) website https://journals.alambiblio.com/ojs/index.php/ajoeee/. Further correspondence on the status of the paper could be done through the journal's website

COPYRIGHT NOTICE

ASIAN JOURNAL OF ELECTRICAL AND ELECTRONIC ENGINEERING

eISSN 2785-8189

9 7 7 2 7 8 5 8 1 8 0 0 2

Published by:

AlamBiblio Press,
PV8 platinum Hill
Jalan Melati Utama, 53100 Kuala Lumpur, Malaysia
Phone (+603) 2713 7308

ASIAN JOURNAL OF ELECTRICAL AND ELECTRONIC ENGINEERING

Volume 5, Issue 1, March 2025

TABLE OF CONTENTS

ASIAN JOURNAL OF ELECTRICAL AND ELECTRONIC ENGINEERING
Vol. 5 No. 1 2025
E-ISSN: 2785-8189

Impact Analysis of Energy-Efficient Demand-Side Management in Six-Bus Systems: Replacing Lighting Loads Based on Consumer Preferences

M. M. Rashid[1], Tasfia Hossain[2], Dhrupadi Barua[2], Mohima Datta[2], Rashedul Islam[2], and Ahmad Mmzr Alazmi[2]

[1]*Dept. of Mechatronics Engineering, International Islamic University Malaysia, Kuala Lumpur, Malaysia*
[2]*Dept. of EEE, USTC, Chattogram, Bangladesh*

*Corresponding author: mdrashedulislam1130@gmail.com

(Received: 21 March 2025; Accepted: 18 April 2025)

Abstract— One of the most important strategies for improving power utilization and lowering total energy usage in distribution systems is energy-efficient Demand Side Management (DSM). Within a substation's load profile, this study assesses the effects of swapping out incandescent lights for consumer-preferred, energy efficient substitutes like LEDs and Compact Fluorescent Lamps (CFLs). Despite certain harmonic distortion issues related to non-linear lighting loads like CFLs, DSM techniques in particular, demand response strategies have been demonstrated to lower power costs, improve power factors, but increase Total Harmonic Distortion (THD). The study evaluates system metrics, including power, THD, power factor, and energy consumption, under different load combinations using MATLAB simulations. The findings of analyzing optimal power flow (OPF) on a six-bus network and modeling a balanced three-phase system show decreases in real power demand, operational losses, and system expenses. Additionally, the economic advantages of DSM interventions are highlighted by differences in Locational Marginal Pricing (LMP) among bus nodes. Results indicate that DSM techniques greatly improve system sustainability and efficiency in power distribution networks by implementing targeted load reduction and energy-efficient lighting.

Keywords: *OPF, THD, Power quality, CFL*

1. INTRODUCTION

Energy efficiency has become a crucial area of focus in power management due to the ongoing increase in global energy consumption and the depletion of fossil fuel resources. Demand Side Management (DSM) techniques have been shown to be successful in lowering costs and conserving energy by providing incentives for customers to switch or reduce their power consumption during periods of high demand. In order to lower total power consumption and enhance system performance, DSM requires replacing traditional high-energy lighting with energy-efficient substitutes like light-emitting diodes (LEDs) or compact fluorescent lamps (CFLs) [1]. Energy consumption is decreased, operational expenses are decreased, and a more balanced and dependable power distribution network is achieved by substituting energy-efficient lights for incandescent ones [1]. According to studies, DSM techniques in distribution systems maximize power flow, guarantee voltage stability, and reduce power losses, making them a workable way to save money and energy. However, using non-linear loads, such as CFLs in place of traditional incandescent lights, results in harmonic distortions, which can alter voltage waveforms and impact power quality. Large-scale lighting changes are therefore possible for operational and financial reasons, as research shows that these power quality problems stay within allowable regulatory bounds

DOI: https://doi.org/10.69955/ajoeee.2025.v5i1.76

[2]. This study examines the effects of switching out incandescent lighting in a substation with consumer-preferred energy-efficient substitutes, with a particular concentration on how it affects cost-effectiveness, power quality, and load flow. This study adds to the increasing amount of research that highlights the advantages of DSM in power distribution networks from an economic and environmental standpoint [3].

2. PROBLEM STATEMENTS

Compact fluorescent lamps (CFLs) and other non-linear lighting loads like LEDs have improved energy efficiency but increased harmonic distortion, particularly third-order harmonics. Harmonic pollution from these devices occurs because they draw current in a way that distorts the voltage waveform, injecting high-frequency currents that create total harmonic distortion (THD) [4-8]. This distortion can lead to increased losses, reduced equipment lifespan, and interference in electronics and transformers not designed for high harmonic levels. Studies show that CFLs can produce THD levels as high as 120% or 72% without filtering, far exceeding the limits set by power quality standards and the much lower distortion of traditional incandescent lights [9-12]. Demand Side Management (DSM) and Demand Response (DR) are being used more and more to control load demand, promote energy efficiency, and lower harmonics to enhance power quality and load profiles, particularly with non-linear loads like LEDs and CFLs. Energy-efficient lighting is encouraged by utilities and Independent Service Operators (ISOs) to improve grid efficiency, prolong equipment life, and reduce maintenance expenses. Aggregators encourage load shifts to balance grid demand and lessen peak load pressure, which aids in coordinating end-user involvement in DR schemes. To improve power quality and equipment longevity, passive or active filters are employed to reduce Total Harmonic Distortion (THD), especially at substations. DSM and DR allow for real-time modifications to optimize grid costs, while Locational Marginal Pricing (LMP) reflects supply-demand restrictions at network locations [13-17]. To provide stable and affordable power distribution, LMP promotes DR interventions during periods of high demand or congestion.

3. METHODS AND PROCEDURES

User-defined load combinations can provide an output load that is applied to a node bus in a six-bus system. Replacing the system load by a percentage reduces output consumption. The lower estimated load is utilized to generate an OPF solution for the system.

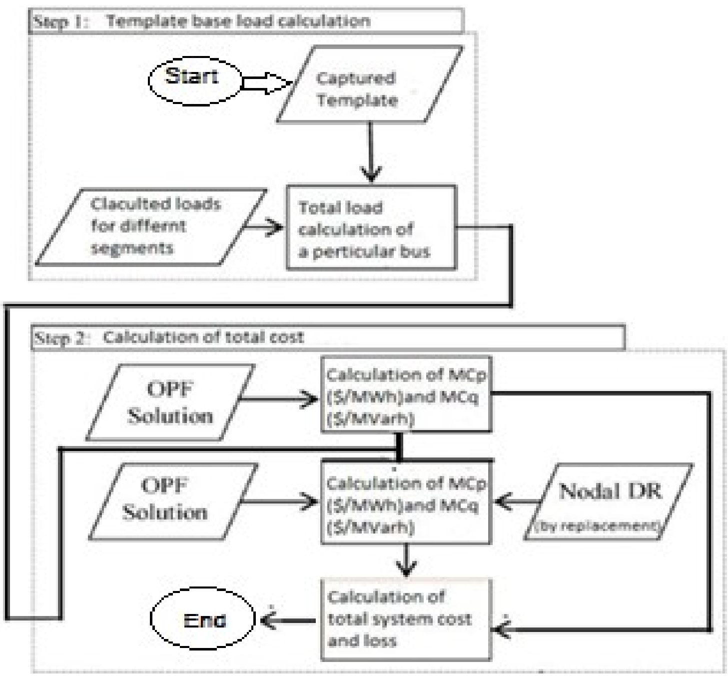

Fig. 1. Process of cost calculation

3.1 Template Base Load Calculation

Data was collected using a computer-controlled setup and saved in a server system before being analyzed [10]. During a capture period, NT samples are obtained as NT-length sequences, as indicated in (1) and (2)

$$v_{acq} = \{v_{acq}(n)\}_{n=1}^{N_T} \quad (1)$$

$$i_{acq} = \{i_{acq}(n)\}_{n=1}^{N_T} \quad (2)$$

Power may be obtained for specific loads, such as CFLs and FLs, with electronic or magnetic ballasts at any time.

$$P_{load} = \frac{1}{N} \sum_{n=1}^{N} v_{tmp}(n) i_{tmp}(n) \quad (3)$$

For any mixed combination, the power can be calculated as

$$P_{mixerload} = \frac{1}{N} \sum_{n=1}^{N} v_{tmp}(n) \left[n_{CFL}(n) * i_{CFL}(n) + n_{EFBL}(n) * i_{EFBL}(n) + n_{MFBL}(n) * i_{MFBL}(n) + \cdots\right] \quad (4)$$

3.2 The Optimal Power Flow (OPF) Solution Formulation of The Network

The OPF solution is calculated using MATPOWER software. To determine the OPF solution, use the following equation:

$$\min_x F(x) = \sum_{i=1}^{N_0} f_P^i(p_g^i) + f_Q^i(q_g^i) \quad (5)$$

Subject to

$$H(x) = 0 \quad (6)$$

$$G(x) \le 0 \quad (7)$$

$$x_{min} \le x \le x_{max} \quad (8)$$

$$x = \begin{bmatrix} \theta \\ V_{min} \\ P_g \\ Q_g \end{bmatrix} \quad (9)$$

The objective function, F, is the sum of each generator's real power cost function. f_P^i and reactive power cost functions, f_Q^i where i=1… and n_g is the number of generators. The equality constraints, H, refer to the nonlinear real and reactive power balancing equations H_P and H_Q, where i=1 and n_b= the number of buses:

$$H = \begin{cases} H_P(\theta, V_m, P_g) = P^i(\theta, V_m) + P_d^i - P_g^i \\ H_Q(\theta, V_m, P_g) = Q^i(\theta, V_m) + Q_d^i - Q_g^i \end{cases} \quad (10)$$

The inequality constraints, G, consist of apparent power flow limits for the from F_f, and to F_t, ends of each line:

$$G = \begin{cases} g_f = |F^f(\theta, V_m)| - F_{max} \\ g_t = |F^t(\theta, V_m)| - F_{max} \end{cases} \quad (11)$$

The optimization vector includes vectors for voltage angles, voltage magnitudes (V_m), and generators' real and reactive power outputs ($P_g$and Q_g)[18-21].

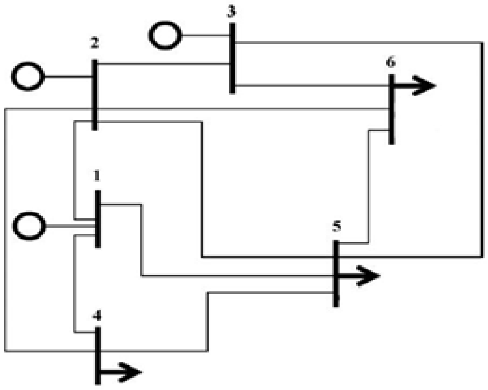

Fig. 2. Diagram of the Six Bus System

4. CASE STUDIES FOR DIFFERENT TYPES OF LOAD COMBINATIONS

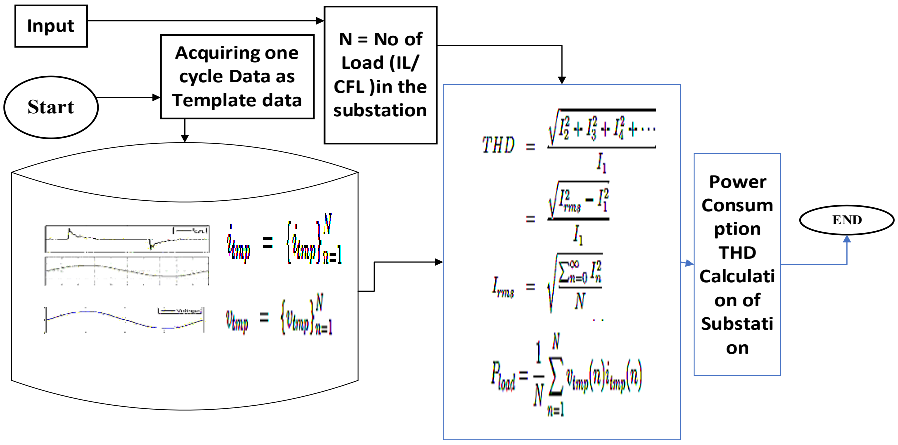

Fig. 3. Mathematical Flow chart

Power, Total Harmonic Distortion (THD), Power Factor (PF), and energy requirements are among the system factors that are assessed for a variety of loads inside a substation in this research. A MATLAB program is used to compute these parameters, and the results are used to optimize the load-serving entities (LSEs) at the nodal level [22].

Table 1: Loads under a 200 MVA transformer

Load Type	Loads under a 200 MVA transformer		
	Unit Power (Watt)	*Quantity* (1000Pcs)	*Total Power* (KWatt)
Fan	60	360	21600
Refrigerator	150	120	18000
AC	1500	30	45000
Washing Machine	500	45	22500
Heater	1000	45	45000
Lamp	60	270	16200
CFL	23	345	7935
TL with MB	40	225	9000
TL with EB	40	165	6600

Assumptions that make on the overall network consideration:

•The system was modelled as a balanced three-phase system, with loads distributed equally across single-phase units.
•Calculations were performed in a single-phase representation for simplicity.

The power parameters can be used to create load-serving entities (LSEs) at the nodal level, incorporating demand response (DR) strategies. DR often involves reducing energy consumption, such as replacing incandescent lamps with energy-efficient options like CFLs. Studies show this leads to notable energy savings, reduced peak demand, lower power losses, and improved system stability.

Possibilities for Demand-Side Management The substitution of energy-efficient substitutes like CFLs for traditional illumination (incandescent lights) is one of the study's major contributions to DSM. Numerous studies have shown that these kinds of changes can result in a significant drop in energy usage, which lowers overall demand and the lowest peak power needs. As reflected in the above table, the percentage reduction in incandescent load due to CFL replacements results in a reduction of both real power demand and overall THD (Total Harmonic Distortion), leading to an improvement in the power factor. Such reductions help improve the efficiency of the overall system and contribute to significant energy savings.

4.1 Optimal Power Flow (OPF) Solution for a Six Bus System

In the Second Step, consideration had been taken for a six bus system shown in the figure (Fig. 2). The details of the system setup are listed in Table III. This phase is essential for calculating the overall cost and loss of the system, depending on the load configurations. Through the use of MATPOWER, the system is assessed under a range of load scenarios, including the effects of load reductions brought on by DSM (switching from incandescent to CFL bulbs). Results of the OPF Analysis: The OPF solution highlights the savings obtained by substituting conventional lamps by displaying the system's overall cost and loss under various demand response scenarios. The predicted loss and cost per hour, along with the load flow statistics, demonstrate how DSM improves system efficiency. The system converges rapidly, and DSM's reduction of the fifth bus's load lowers operating expenses and improves system dependability. All the other parameters were taken from the reference [23].

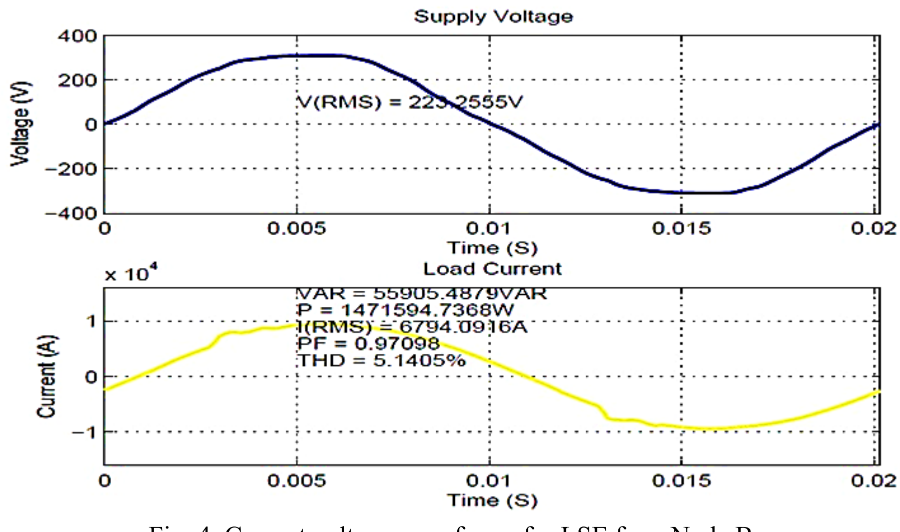

Fig. 4. Current voltage waveforms for LSE for a Node Bus

4.2 Units Load Reduction at the Nodal Level

Every 25% replacement of CFLs for incandescent lamps results in a decrease in load at the nodal level. A progressive reduction in the overall system power and an increase in the power factor may result from this demand response. The consequences of the load reduction are shown in Energy consumption and system costs, which are greatly decreased when traditional incandescent lamps are swapped out with more energy-efficient models, like

CFLs, in the substation's load profile. By putting DSM techniques into practice, especially at the consumer level, utilities can improve the system's overall power quality, minimize operating losses, and lessen demand. The Current voltage waveforms for LSE for a Node Bus are shown in Figure 4.

5. OUTCOMES AND EVALUATION

The results of this study are consistent with other studies on DSM and energy efficiency, suggesting that these tactics can be very important for maximizing energy use and promoting sustainable energy systems. The system output data also illustrates how DSM affects the overall real and reactive power as well as the operational cost of the system. In Table II, all variations in the real and reactive power, along with the costing per hour, are included. Also, the LMP analogy for different calculations is shown in the graph (Fig. 5).

Table 2: Load Replacement by Percentage for Demand Response

Load Reduction	Parameter for Demand Response				
	Real Power (MWatt)	*Reactive Power* (MVAR)	*Total Total* (MAmp)	*THD* (pc)	*PF* (pc)
No Reduction	147.16	5.59	6.79	5.14	0.971
25 pc Reduction	144.77	5.59	6.69	6.25	0.97
50 pc Reduction	142.39	5.59	6.58	7.39	0.969
75 pc Reduction	137.48	5.59	6.28	9.92	0.98
100 pc Reduction	137.43	5.59	6.26	9.98	0.98

The table summary shows that the total cost per hour is lower for Demand Response (DR) at any node, even when energy-efficient alternatives are used to replace lighting demands (as shown in Table II). Though it stays within the bounds specified by the IEEE 519 standard, this modification can cause a slight decline in the network's power quality. The Locational Marginal Pricing (LMP) at each node changes considerably across different bus points, according to the graphical study. Nodes two and three maintain a constant LMP value, whereas other buses, like bus five, experience a decline in LMP value as load is reduced. It's interesting to see that when the load drops, the LMP at the generator on one bus somewhat increases. In conclusion, the overall system cost will be reduced as DSM activities replace incandescent lights with energy-efficient lighting; however, the LMP at various network locations will not show consistent reductions.

The calculated data illustrates the hourly variation of Locational Marginal Prices (LMP) and their impact on economic metrics such as the difference with retail tariffs and objective value throughout the day. During early hours (1:00–6:00), the LMP remains relatively stable with low price differences compared to the retail tariff, resulting in modest objective values between $32,000 and $33,000. However, as demand increases from 7:00 onwards, LMP values escalate, especially during peak hours (12:00–17:00), where prices and objective values rise significantly, reflecting increased energy consumption costs. Notably, from 18:00 to 22:00, the LMP range widens drastically, with maximum LMP values spiking to above $300/MVA-hr, resulting in negative differences with the retail tariff, indicating a possible surplus generation scenario. This leads to exceptionally high objective values, peaking at $82,105 during the 19:00 hour. These trends reflect typical demand-supply dynamics and the importance of strategic DSM measures to optimize energy usage, particularly during high-price intervals.

The graph in Figure 6 shows the effects of varying levels of power reduction on key electrical parameters for an industrial system. As the percentage reduction in real power increases from 0% to 100%, real power output decreases steadily from 147.16 MW to 137.43 MW. Interestingly, reactive power remains constant at 5.59 Mvar across all reduction levels, indicating that reactive power demand is independent of the real power reduction in this scenario.

The total current also decreases progressively from 6.79 A at 0% reduction to 6.26 A at 100% reduction, aligning with the reduced real power consumption. However, Total Harmonic Distortion (THD) increases significantly from 5.14% to 9.98%, suggesting that power quality may deteriorate as reductions in real power are applied. The power factor (Pf) starts at 0.971 and slightly improves to 0.98 at higher reduction levels, likely due to the consistent reactive power and decreased real power. These observations emphasize the trade-offs between energy savings, power quality, and system efficiency in Demand-Side Management (DSM) strategies

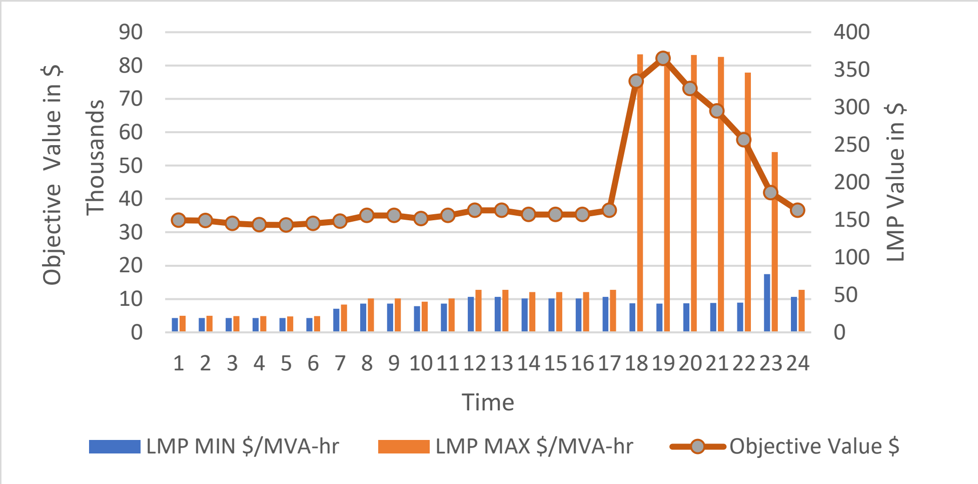

Fig. 5. LMP (max/ min) Vs objective values for a Node Bus

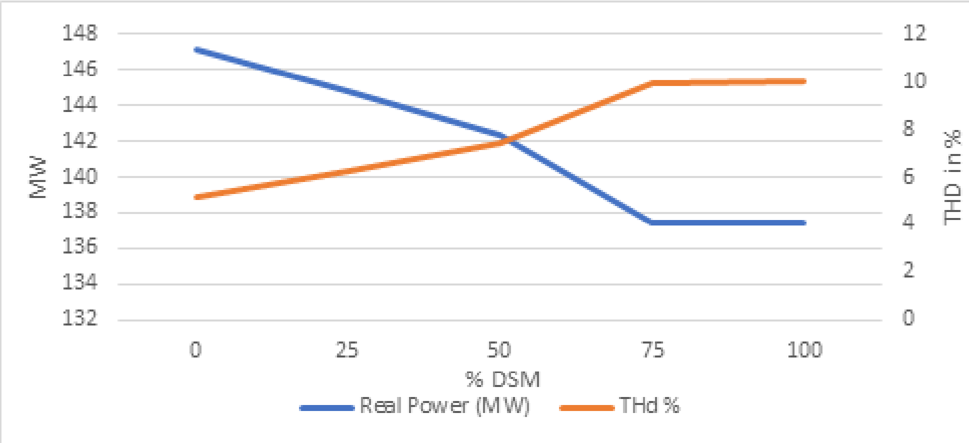

Fig. 6. Quality Vs objective values for a Node Bus

.

6. CONCLUSION

The paper suggests a novel method for modelling loads using waveform templates. Real-time waveforms that have been acquired undergo manipulation to create the templates. The power quality parameters of a distribution system with various load combinations are ascertained using these templates. It is discovered that the individual current waveform of CFL contains THD of greater than 12%. The THD of an electronic ballast is close to 20%. The CFL and electronic ballast each have extremely significant individual harmonic distortions. The overall power scale shrinks to about 20% of the lamp load when a CFL is used in place of a lamp. Nevertheless, the leading power factor drops from unity to 0.57. However, the power quality does not change much when an electronic ballast is used in place of a tube light with a magnetic ballast. Even so, it raises the power factor from a lagging 0.57 to nearly unity. The THD is not greatly impacted when switching the ballast for tube light loads from an electronic ballast to a normal magnetic ballast.

REFERENCES

[1] O. Popoola, J. Munda, and A. Mpanda, "Residential lighting load profile modelling," Energy Build, vol. 90, pp. 29-40, Mar. 2015, https://doi.org/10.1016/j.enbuild.2015.01.005

[2] Mmzr Alazmi, MMR, "Analysis and Optimization of Fuzzy Logic Based MPPT for Grid Connected Photovoltaic System", AJoEEE, vol. 2, no. 2, pp. 28-37, Oct. 2022, https://doi.org/10.69955/ajoeee.2022.v2i2.36

[3] W. J. Jones, "The lighting load-its characteristics and development, "Journal of the Institution of Electrical Engineers, vol. 83, no. 501, pp. 289-299, Sep. 1938, https://doi.org/10.1049/jiee-1.1938.0145

[4] Syed Munimus Salam, Nur Mohammad, Muhammad Mahbubur Rashid, "Quantifying demand-side management in sustainable grid networks by industrial load flexibility with variable inertia flywheel induction motors", e-Prime-Advances in Electrical Engineering, Electronics and Energy, Vol 11, 2025.https://doi.org/10.1016/j.prime.2024.100890

[5] A. Powers and M. Saad, "Building Energy Use: Modeling and Analysis of Lighting Systems-A Case Study," Sustainability, vol. 14, no. 20, p. 13181, Oct. 2022.https://doi.org/10.3390/su142013181

[6] S. M. Salam and M. M. Rashid, "A new approach to analysis and simulation of flywheel energy storage system," 8th International Conference on Mechatronics Engineering (ICOM 2022), Online Conference, Kuala Lumpur, Malaysia, 2022, pp. 90-94. https://doi.org/10.1049/icp.2022.2271

[7] S. Adhigunarto, E. Mulyana, and W. Surya, "The Analysis of Harmonics on LED Lamps," IOP Conf Ser Mater Sci Eng, vol. 384, p. 012061, Jul. 2018.https://doi.org/10.1088/1757-899X/384/1/012061

[8] SM Salam, Nur Mohammad, "Cost-Centric Energy Management of a Test Grid System Considering Load Flexibility for DSM", International Journal of Electrical and Electronic Engineering & Telecommunications, Vol 13, Issue 2, 2024.https://doi.org/10.18178/ijeetc.13.2.125-134

[9] C. Brusil, H. Arcos, F. Espin, and C. Velasquez, "Analysis of Harmonic Distortion of LED Luminaires Connected to Utility Grid," in 2020 IEEE ANDESCON, IEEE, Oct. 2020, pp. 1-6. https://doi.org/10.1109/ANDESCON50619.2020.9272004

[10] S. M. Salam and N. Mohammad, "Load Flow Analysis of a Six Bus System for a Bulk Scale Replacement of Conventional Lighting Loads in a Distributed Network," 2020 IEEE Region 10 Symposium (TENSYMP), Dhaka, Bangladesh, 2020, pp. 831-834. https://doi.org/10.1109/TENSYMP50017.2020.9230818

[11] G. McLorn, D. Laverty, D. J. Morrow, and S. McLoone, "Load and harmonic distortion characterization of modern low-energy lighting under applied voltage variation," Electric Power Systems Research, vol. 169, pp. 124-138, Apr. 2019. https://doi.org/10.1016/j.epsr.2018.12.029

[12] A. Sardar, S. U. Khan, M. A. Hassan, and I. M. Qureshi, "A demand side management scheme for optimal power scheduling of industrial loads," Energy Systems, vol. 14, no. 2, pp. 335-356, 2023. https://doi.org/10.1007/s12667-022-00510-x

[13] S. M. Salam, M. I. Uddin and M. R. Bin Moinuddin, "Impact Analysis of Large Number of Non-Linear Lighting Loads on Power Quality in Distribution Network," 2019 4th International Conference on Electrical Information and Communication Technology (EICT), Khulna, Bangladesh, 2019, pp. 1-5. https://doi.org/10.1109/EICT48899.2019.9068811

[14] S. Tangi, D. N. Gaonkar, A. S. Veerendra, and R. Shivarudraswamy, "Time Series-Based Load Flow Simulation Algorithm for Distributed Generation in Distribution Networks," in EEPES 2024, Basel Switzerland: MDPI, Jul. 2024, p. 11. https://doi.org/10.3390/engproc2024070011

[15] S. M. Salam, M. J. Uddin, and S. Hannan, "A new approach to develop a template-based load model that can dynamically adopt different types of non-linear loads," in ECCE 2017 -

International Conference on Electrical, Computer and Communication Engineering, IEEE, Feb. 2017, pp. 708-712. https://doi.org/10.1109/ECACE.2017.7912996

[16] MM Rashid, SY Salam, MY Ali, S Yvette, "Implementation and performance analysis of a controlling system of a water pump coupled with VIF", AIP Conference Proceedings 3161 (1), 2024. https://doi.org/10.1063/5.0229874

[17] J. A. Momoh, M. E. El-Hawary, and R. Adapa, "A review of selected optimal power flow literature to 1993 part i: nonlinear and quadratic Programming Approaches," IEEE Transactions on Power Systems, vol. 14, no. 1, pp. 96-103, 1999. https://doi.org/10.1109/59.744492

[18] S. M. Salam and N. Mohammad, "Analyze the Impact of Demand Side Management on Grid Power for an Isolate Zone in a Sustainable IEEE 14 Bus System,"2021 International Conference on Information and Communication Technology for Sustainable Development (ICICT4SD)", Dhaka, Bangladesh, 2021, pp. 16-20. https://doi.org/10.1109/ICICT4SD50815.2021.9396975

[19] R. D. Zimmerman, C. E. Murillo-Sánchez, and R. J. Thomas, "MATPOWER's extensible optimal power flow architecture," in 2009 IEEE Power and Energy Society General Meeting, PES '09, IEEE, Jul. 2009, pp. 1-7. https://doi.org/10.1109/PES.2009.5275967

[20] Munimus Salam, S., & Mahbubur Rashid, M. (2023). Performance Analysis of a Designed Prototype of a Motor Coupled Variable Inertia Flywheel System. Malaysian Journal on Composites Science and Manufacturing, 12(1), 62-72. https://doi.org/10.37934/mjcsm.12.1.6272

[21] M I Uddin, K S dsd Huq, S M Salam "Performance Analysis of a Newly Designed DC to DC Buck-Boost Converter", AJoEEE, vol. 2, no. 2, pp. 38-42, Oct. 2022. https://doi.org/10.69955/ajoeee.2022.v2i2.38

[22] B. F. W. Allen J. Wood, Power Generation, Operation, and Control . John Wiley & Sons, Inc., 1996.

[23] S. M. Salam, N. Mohammad and F. Hossain, "A new approach to Analysis the Impact of Demand Side Management for Temperature Control Load Consideration in a Test Bus System, "2021 5th International Conference on Electrical Information and Communication Technology (EICT)", Khulna, Bangladesh, 2021, pp. 1-6. https://doi.org/10.1109/EICT54103.2021.9733717

ASIAN JOURNAL OF ELECTRICAL AND ELECTRONIC ENGINEERING
Vol. 5 No. 1 2025
E-ISSN: 2785-8189

Energy Efficiency Optimization in Algorithm for RIS-Assisted UAV-Enabled MEC-IoT Networks

Areeg Ali Elnaim[1*], Amin Babeker[1], and Ziane Ataoua[2]

[1]*College of Engineering and communication, Alneelain University, Khartoum, Sudan*
[2]*Dept of Electrical Engineering Alneelain University, Khartoum, Sudan*

*Corresponding author: Areeg446@gmail.com

(Received: 5 July 2025; Accepted: 25 July 2025)

Abstract—The combination of drones and smart reconfigurable surfaces (RISs) is becoming increasingly important for improving energy efficiency and wireless communication performance in Internet of Things (IoT) networks. This research focuses on developing an iterative optimization algorithm based on the fmincon algorithm in MATLAB. Sensing and transmission parameters are updated simultaneously at each iteration to achieve maximum energy efficiency. The algorithm starts with initial values. To optimize the energy efficiency of a system integrating a drone that provides mobile edge computing (MEC) services to IoT devices, the proposed system takes into account several critical factors, including drone trajectory optimization, optimal bit allocation between local and drone processing, and phase shift optimization in smart reconfigurable surfaces. The goal is to maximize overall energy efficiency by jointly optimizing these elements through a novel algorithm that alternates between optimizing the smart reconfigurable surfaces' phase shifts, the drone trajectory, and bit allocation. Simulation results demonstrate that the proposed solution significantly outperforms other measurement approaches in terms of energy efficiency, while examining the impact of variables such as the number of users, the reflectance elements of reconfigurable smart surfaces, and base station antennas on system performance. In conclusion, this research presents a novel approach to enhancing energy efficiency in RIS-enabled and drone-enabled MEC systems for IoT networks, achieving significant improvements over existing methods

Keywords: *Cognitive radio networks (CRNs), unmanned aerial vehicles (UAVs), Reconfigurable Intelligent Surfaces (RIS), Mobile Edge Computing (MEC), Energy Internet of Things (IoT)*

1. INTRODUCTION

The rapid development of the Internet of Things (IoT), data traffic will increase completely, necessitating a large amount of spectrum. Cognitive radio (CR) technology has been proposed as a solution to the spectrum scarcity problem[1] .It improves spectrum efficiency. In cognitive IoT, secondary IoT devices can coexist with nearby primary IoT devices on the same spectrum while ensuring that secondary users' interference is kept to a minimum The utilization efficiency of the licensed spectrum can be increased. Integrating ground-based and air-based networks is one of the challenges in building a six-generation (6G) communication system[2] . Unmanned aerial vehicle (UAV) assisted communication has been extensively researched in civil and military applications due to its numerous benefits, including high maneuverability [3], on-demand deployment, and so on. UAVs can be used as aerial base stations, providing wireless service to ground users Because of the bottleneck in battery technology [4], the UAV system's operating time will be reduced. Therefore, it is urgent to improve the energy efficiency (EE) of the UAV system. The UAV is deployed as an aerial base station, providing wireless services to ground users. The UAV's trajectory, bandwidth allocation, and user communication scheduling are optimized to maximize EE while meeting user quality-of-experience (QoE) requirements Consider a spectrum sharing system in which the UAV circles the PU transmitter and detects its status using spectrum sensing. When detected to be idle, UAVs can use the licensed spectrum for short packet communications [5]. Because of the UAV's high

DOI: https://doi.org/10.69955/ajoeee.202x.v5i1.78

altitude, wireless channels between and ground nodes are assumed to be links. For micro rotary-wing UAVs that are typically powered by batteries, EE is an important performance metric to consider. First, we calculate the effective throughput of the UAV communication system by taking into account the effect of imperfect sensing and packet error rate [6]. The average energy consumption of the UAV system is then calculated, which includes hovering energy, propulsion energy, and communication energy. The EE is the ratio of average throughput to average power consumption [7]. We aim to maximize EE by designing the packet error rate, sensing duration, normalized sensing threshold, and the UAV's transmit power.

The packet error rate, sensing duration, normalized sensing threshold, and UAV transmit power are all optimized together to maximize the UAV system's EE [8].

The integration of (UAVs) and Reconfigurable Intelligent Surfaces (RIS) marks a significant step forward in the design of next-generation wireless communication networks [8]. UAVs, with their mobility and flexibility, offer a dynamic platform for improving wireless coverage and capacity, especially in challenging environments. Simultaneously, RIS technology provides a novel method of controlling the propagation environment [9], enabling intelligent manipulation of electromagnetic waves to improve signal strength and reduce interference In the context of Mobile Edge Computing (MEC) [10], which needs to bring computation and storage closer to end users, the collaboration between UAVs and RIS has the potential to significantly improve the efficiency and reliability of data processing and transmission in Internet of Things (IoT) networks. However, optimizing such a complex system presents numerous challenges [11], particularly in terms of energy efficiency, which is critical given UAVs' limited power resources and need for long-term operation without frequent battery replacements or recharges [12].

In This paper the objective: Develop a comprehensive optimization framework to enhance energy efficiency in a RIS-assisted UAV-enabled MEC system.

2. RELATED WORKS

. This study focuses on using (UAVs), Reconfigurable Intelligent Surfaces (RIS), and Multi-Access Edge Computing (MEC) to improve energy efficiency in wireless networks. Several studies have investigated these approaches separately or in combination to improve wireless network performance.

In (UAVs) The UAVs have shown to be a valuable tool for increasing energy efficiency and expanding wireless coverage. For example, Ghamari et al. (2022) conducted a review of UAV applications in civil domains, emphasizing their benefits in terms of wireless coverage and spectrum efficiency. Research has mostly focused on optimizing UAV trajectories and resource utilization to reduce energy consumption and Reconfigurable Intelligent Surfaces (RIS)

RIS is a novel breakthrough in wireless communication that provides new techniques to regulate the propagation environment. In a comprehensive analysis, Ahmed et al. (2024) underlined that RIS improves signal strength, decreases interference, and broadens wireless communication possibilities, making it a potential solution for future networks (MEC).

MEC dramatically improves wireless network performance by lowering latency and increasing data processing efficiency. Narayanan et al. (2020) examined important achievements in MEC for industrial IoT applications, noting its critical role in enhancing data transmission reliability, especially when linked with UAV and RIS technologies, and challenges and improvements in energy efficiency.

Despite tremendous advances in these fields, increasing energy efficiency remains a serious problem. Key concerns include UAVs' limited energy resources and the necessity for long-term operations without regular battery replacement. To solve these difficulties, this research provides a comprehensive system that includes UAVs, RIS, and MEC. The suggested solution uses iterative algorithms and gradient-based approaches to optimize system parameters over several time periods, with the goal of significantly improving energy efficiency.

The associated works stress the need for ongoing research to increase energy efficiency in integrated wireless systems. Building on previous contributions, this study presents a novel paradigm that may be used to real-world settings, paving the way for more sustainable and efficient wireless communication systems.

TABLE 1. Abbreviation for related works.

REF	*PAPER*	*Field*	*Main Goals and Results*
[9] 2024	*Active Reconfigurable Intelligent Surface es: Expanding the frontiers of wireless communication.*	*(RIS)*	*Comprehensive review of RIS technology and its potential to improve signal strength and reduce interference in wireless communication.*
[13] 2023	*Joint optimization of resource Allocation, phase shift, and UAV trajectory for Energy Efficient RIS-Assisted UAV-Enabled MEC.*	*EE optimization*	*Optimization resource allocation, phase shift, and UAV trajectory to maximize EE in RIS-assisted UAV-enabled MEC.*
[11] 2023	*Reconfigurable intelligent surface for physical layer security in 6G-IOT*	*physical layer security*	*Improving security in 6G-IOT networks using RIS,*
[1] 2022	*Throughput optimization of interference limited cognitive Radio Radio-based IOT Network.*	*IOT Networks*	*Enhancing spectrum efficiency by optimizing throughput in cognitive Radio Radio-based IOT Networks.*
[3] 2022	*UAV communications for civil Applications*	*UAV communications*	*Reviewing the civil applications of UAVs and their benefits in enhancing wireless coverage and spectrum efficiency.*
[10] 2020	*Key Advances in pervasive Edge computing for Industrial IOT.*	*Edge computing*	*Enhancing efficiency and reliability of data transmission in industrial IOT networks through edge computing technologies.*
[2] 2019	*IOT Enabled wireless sensor Network for physiological data Acquisition.*	*Wireless sensor networks.*	*Improving physiological data acquisition using IOT-enabled wireless sensor networks.*
This Paper 2025	*Energy Efficiency optimization in cognitive Radio Networks RIS assisted UAV Enabled MEC system.*	*Energy Efficiency In Networks.*	*Proposing a comprehensive frame work to optimize Energy Efficiency by integrating UAVs, RIS, MEC.*

3. SYSTEM MODEL

This system model describes the integration of (UAVs), Reconfigurable Intelligent Surfaces (RIS), The model encompasses the operational parameters and interactions between these components, focusing on energy efficiency optimization.

4. OPTIMIZATION OF THE ORIGINAL SYSTEM

In this section, we focus on optimizing the performance of the UAV system supported by the reconfigurable intelligent surface (RIS) in terms of energy efficiency

The goal is to maximize the (EE) by adjusting various system parameters.

4.1 Energy Efficiency Optimization

The objective function is the function we aim to r maximize (EE) of the system.

The energy efficiency of the UAV system can be calculated using the following equation:

$$EE = \frac{1-q\left(x(2)-1)\sqrt{\frac{x(1).fs}{w}}\right).\left(M-x(1)\right).\left(1-x(4)\right)}{x(1).ps+\left(M-x(1)\right).(x(3)+pc)+\frac{mUAV.g}{\sqrt{2\pi.Nu.p}}+other\ term} \quad (1)$$

x1 represents the sensing duration, x2 the sensing threshold, x3 the UAV transmit power, x4 the packet error rate, q the gaussian q-function, fs is the sampling frequency, W is the bandwidth, M is the number of symbols [14], pc circuit power, ps represents sensing power, g is the gravitational acceleration, Nu is the number of rotors, and mUAV is the UAV's mass [15] .

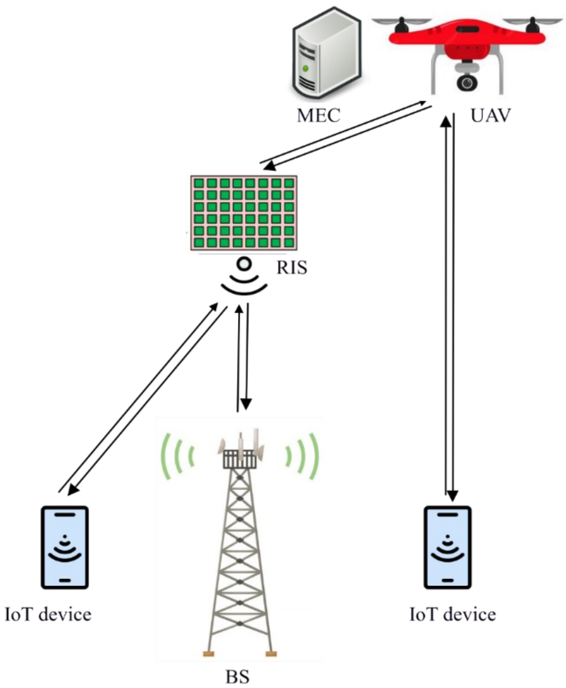

Fig 1: System Model illustrating UAV, RIS, and MEC -Assisted communication for IOT

5. CONSTRAINTS

Constraints are important in any optimization problem because they ensure that the optimal solutions meet particular requirements or limitations. To optimize the energy efficiency of a UAV system supported by a Reconfigurable Intelligent Surface (RIS), certain restrictions must be considered to ensure that the system operates properly and efficiently.

5.1 Detection Probability

The detection probability refers to the likelihood of successfully detecting the signal. To achieve consistent performance, the detection probability must be high. We utilize the Gaussian Q-function to get the detection probability:

$$pd = Q\left(k - ys - 1\right)\sqrt{\frac{nfs}{w(2ys+1)}}\Bigg) \quad (2)$$

Where:

Q is the Gaussian Q-function, which represents the likelihood that a Gaussian random variable will surpass a given value w. (SNR), fs is the sampling frequency ys, and w is the bandwidth.

We want to achieve a detection probability of at least 0.9 for effective signal detection.

False alarm likelihood pf

$$pf = Q\left((k-1)\sqrt{\frac{nfs}{w}}\right) \tag{3}$$

where κ is the normalized threshold of the energy detector, fs is the sampling frequency [13], Q(x) is the complementary distribution function of the standard Gaussian, γs is the signal-to-noise ratio (SNR) of the primary signal at the UAV [14]

$$\gamma s = \beta 0Pp / (r\alpha\ s\ \sigma 2\ u) \tag{4}$$

where σ2 u is the noise power.

5.2 *Sensing* duration

The sensing duration is the time period during which the UAV collects information [16]. It must be within reasonable limits to ensure system efficiency:

$$Ts = (1+\gamma.\log(d)).\ (1+\alpha.\frac{pt}{pt\ max}).\ (1+\lambda.\frac{I}{pt}).\ (1+\beta.\frac{1}{1+exp\ (-\delta.d)} \tag{5}$$

γ the factor adjusts the influence of distance, while α adjusts the effect of transmit power. β represents the environmental effect, while δ represents the effect over distance.

5.3 *.Sensing Threshold*

The sensing threshold is the signal level that is deemed sufficient to detect the signal. It must fall inside specified boundaries:

$$\Theta = \eta.\log\ (1+\frac{pt}{\sigma}).\ (1+\zeta.\frac{d}{R}).\ (1+\alpha.\frac{I}{pt}).\left(1+\beta.\frac{1}{1+exp\ (-\gamma.SNR)}\right).(\ 1+\delta.E) \tag{6}$$

η.log (1 + pt/σ) This section depicts the influence of transmission power pt in relation to noise. σ is heavily influenced by the signal-to-noise ratio in the communication environment. (1+ ζ.d/R) reflects the effect of distance (d) and R. The efficacy of communication diminishes.

5.4 *UAV Transmit Power*

The transmit power refers to the energy utilized by the UAV to send the signal. To avoid excessive energy use and ensure energy efficiency, it must adhere to particular constraints.

$$Pt = (\frac{\alpha}{\beta+\gamma}).\ (1+\log\ (\frac{d}{R})).\ (1+\ \delta.\ \exp\ (-\epsilon.\ d)).\ (1+\zeta.SNR).\ (1+\eta.\frac{I}{pt}).\ (1+\text{ɵ}.E) \tag{7}$$

α, β, and γ are scaling parameters, while δ and ϵ are adjustment parameters.

5.5 *Packet Error Rate (PER)*

The packet error rate is the percentage of packets that do not arrive at their intended destination. To ensure the quality of communication, it must be within reasonable boundaries.

$$pe = \frac{\mu}{1+\omega.Pt}.(1+\zeta.\frac{pe^{inter}}{pt}).\ (1+\mathcal{E}.\log(\frac{d}{R})) \tag{8}$$

μ, ω, ζ , Ɛ constants adjusted for different effects.

6. COMMUNICATION MODEL

Tthe channel gain between the UAV and the RIS at time slot n can be given by:

$$hRu[n] = \sqrt{pdRu^{-2}[n]}\left[1, \dots, e^{-j\frac{2\pi}{\lambda}(M-1)d\varphi Ru[n]}\right] \tag{9}$$

where ρ is the path loss at the reference D0 =1 m, d is the antenna separation; λ is the carrier wavelength; RU[n] is the cosine of the AD of the signal from the RIS to the UAV at time slot n [17].

the channel gain from the IoT device to the UAV at time slot n can be expressed as:

$$Hiu[n] = \sqrt{p\ d^{-\epsilon} iu\ [n]}giu \tag{10}$$

the IoT device at timeslot n; ε is the pathloss exponent and giu represents the random scattering component [18]. For the communication links from the IoT devices to the RIS [19]. we assume that they are Rician fading channels.

the channel gain between the IoT device and the RIS at time slot n can be given by:

$$hiR\ [n] = \sqrt{\mathrm{p\ d^{-\gamma}iR[n]}}\left(\sqrt{\frac{\beta}{1+\beta}}\ \mathrm{hiR^{loS}} + \sqrt{\frac{1}{1+\beta}}\mathrm{hiR^{NLoS}} \right) \tag{11}$$

the distance between the IoT device and the RIS is dir., γ denotes the path loss exponent; β represents the Rician factor; h loss and N loss are the Loss component and N Loss component [20], respectively For h loss .

7. SYSTEM OPTIMIZATION AFTER INTEGRATING WITH RIS AND MEC

In this section, we will optimize the system following its integration with Reconfigurable Intelligent Surface (RIS) and (MEC) [21]. The goal is to increase the system's energy efficiency (EE) by adding these technologies and modifying the necessary system parameters.

7.1 Formulating the Optimization Problem after Integration

Objective Function

As stated in the first section, the goal is to maximize (EE). The integration of RIS and MEC increases the system's complexity [22], but the goal function can be stated similarly, accounting for the additional impacts.

Modified Objective Function

Following the integration of RIS and MEC, the goal function is adjusted to take into account the additional features, such as increased signal quality from RIS and reduced latency from MEC. The modified objective function may be stated as:

$$EE(X) = \frac{R(x)-p(x)}{p(x)} \tag{12}$$

Rx: Data rate (throughput) after optimization, and P(x): System power consumption after optimization.

8. MODIFIED CONSTRAINTS

In current UAV systems, integrating technologies such as Reconfigurable Intelligent Surface (RIS) and (MEC) has the potential to significantly improve overall system performance [22]. However, in order to properly utilize new technologies, traditional system limits must be revised. These updated limitations provide an ideal mix of performance, efficiency, and sustainability while adhering to legal and operational standards.

Modified constraints are important because they can increase energy efficiency, signal quality, and reaction time, which includes:

8.1. Accurate Signal Detection: Increasing the detection probability to achieve improved signal recognition accuracy[23] and reduce interference mistakes.

8.2. Improving Response Time: Using MEC capabilities to reduce data processing response time and enhance system performance in time-sensitive applications.

8.3 .Improving Signal Quality: Using the RIS system's reflection angles to manage signal direction and quality.

8.4. Compliance with Legal restrictions: Ensuring that UAV transmission power is within legal and operational restrictions [23].

1 .Detection Probability Constraint:

The detection probability of a system relates to its capacity to detect signals accurately in the face of noise. A high detection probability is required to avoid missing key signals or misidentifying them as noise. This limitation ensures that the system's signal detection remains highly efficient.

$$Pd = Q\left(\frac{\gamma - Tth}{\sqrt{\frac{N0}{2T}}}\right) \tag{13}$$

Sensing Duration (T): The time required for the system to detect a signal. Longer sensing times can improve detection accuracy but may cause delays.

Sensing Threshold: The threshold value used to assess whether a detected signal is meaningful or not. Increasing this amount may result in fewer false detections.

Signal-to-Noise Ratio (SNR, γ) is the ratio of signal strength to background noise. High SNR ratios suggest clearer signals and consequently better detection, while N0 denotes the power density of noise in the signal.

2 .MEC Constraints

(MEC) systems process data at the network edge, close to users, to minimize latency and boost efficiency. This restriction ensures that the latency caused by data processing in MEC does not exceed a predetermined level, hence maintaining service quality.

$$D\ total\ = \frac{L}{R}\cdot\left(1+\sum_{i=1}^{M}\frac{p\ useri}{R\ network\ i}\cdot\delta i\right)+\sum_{k=1}^{N}\left(\frac{Lk}{Ck}\cdot\left(1+\frac{Ntasks\ k}{\mu k}\right)\right) \tag{14}$$

L is the magnitude of the data being communicated, and R is the network's transmission rate. M represents the number of users in the system. δ Interference between users represents the number of edge servers.

9. ANALYSIS AND PROBLEM FORMULATION

In this research, we seek to maximize the energy efficiency of an integrated system that includes a drone-enabled MEC and a reconfigurable smart surface (RIS) to increase connectivity to a variety of Internet of Things (IoT) devices. Improving energy economy and lowering overall system power consumption to ensure fast and reliable communications strikes a balance between performance and uptime.

Initialized parameters are bandwidth, sampling frequency, SNR of the primary signal at the UAV, transmit power, path loss exponent, noise power at the UAV and SGR, UAV mass, and so on. These parameters are important in defining the physical characteristics of the UAV, channel models, and the energy consumption model.

System Parameters for RIS-Assisted UAV-Enabled MEC System: The number of RIS elements, the number of IoT devices, the mission period, the UAV height, the maximum UAV speed, and the CPU frequency for IoT and UAV are all defined. These parameters are necessary for the MEC system's operation.

Initial Positions and Channel Models: The UAV, RIS, and IoT devices' initial positions have been set. Channel models between UAV-RIS, IoT-UAV, and IoT-RIS are

Defined using these positions.

Optimization Variables:

Variables used for optimization: Variables like the local computation bits, UAV computation bits, and phase shifts (theta) are all initialized, and Objective function

The objective function seeks to maximize energy efficiency (EE). The function takes into consideration many variables, such as sensing duration; furthermore, sensing threshold, UAV transmit power, and packet error rate. The function is defined by utilizing system parameters and optimization variables; moreover, the constraint (Pd) ensures that the probability of detection exceeds or equals 0.9. This is modeled as a nonlinear constraint.

The energy efficiency is calculated after integrating the system with the assisting system using the following iteration:

$$EE = \frac{\sum_{n=1}^{N} L[n]}{\sum_{n=1}^{N} E[n]} \quad (15\text{ a})$$

L is the total number of bits processed locally and, on the UAV,E is the total energy consumed, including local processing, UAV operation, and its movement [24] .

$$\text{s.t.}|\theta m[n]| = 1 ,\forall m \in M, n \in N , \quad (15b)$$

$$q[1] = q0, q[N + 1] = qF, \quad (15c)$$

$$\|\upsilon[n]\| \leq V\, Max, \forall n \in N, \quad (15d)$$

$$\frac{l\, i^{loc}[n] c\, i}{t} \leq F\, i, \forall i \in I, n \in N, \quad (15e)$$

$$\frac{\sum_{i=1}^{I} li^{UAV}[n] ci}{t} \leq F\, UAV, \forall n \in N \quad (15f)$$

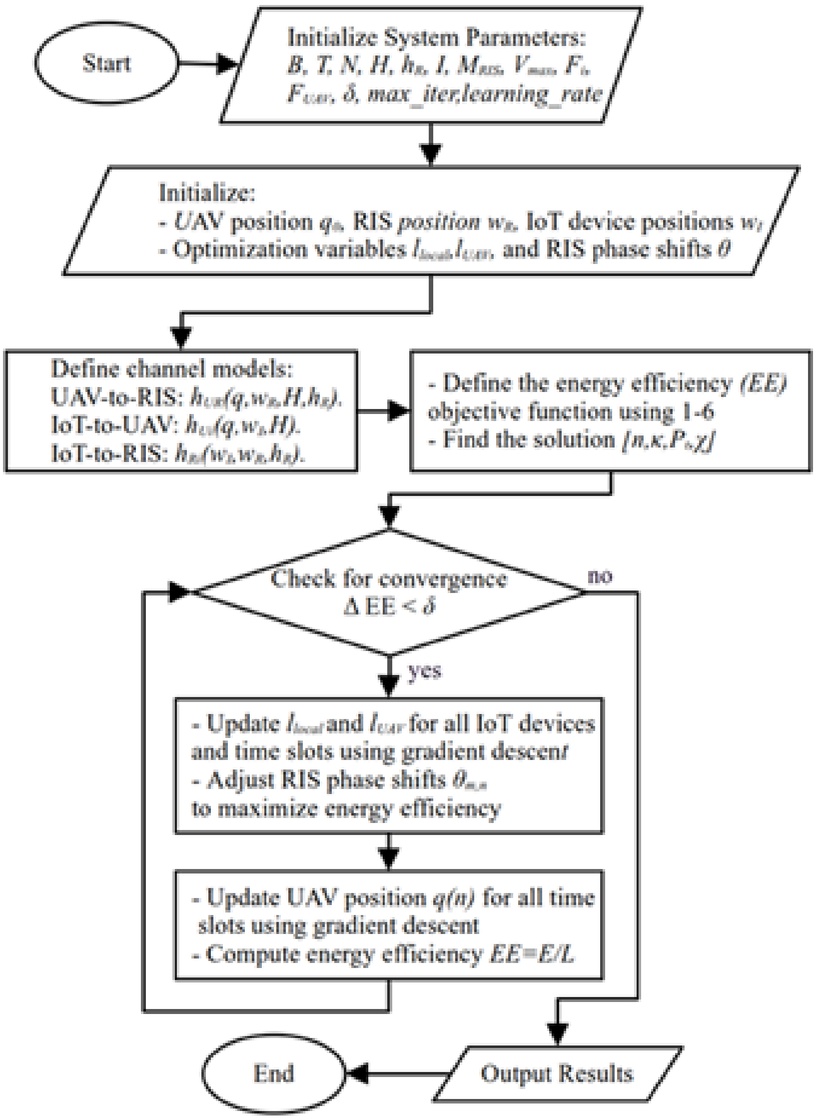

Fig 2: Flowchart for Energy Efficiency optimization in UAV-RIS IOT Systems

Constraint (15b) represents the viable set of RIS phase shifts. Constraint (15c) refers to the UAV's starting and ultimate horizontal locations. Constraint (15d) specifies that the speed of the UAV must be less than its maximum speed. Fi and FUAV represent the maximum CPU frequencies of IoT device i and the UAV, respectively. Constraints (15e) and (15f) require that the workloads of IoT devices and UAVs not exceed their maximum CPU frequency.

10. SOLUTIONS OF THE FORMULATED PROBLEMS

The Iteration Index is a fundamental aspect of any iterative optimization algorithm. It plays a crucial role in tracking and guiding the optimization process toward reaching the best possible solutions. the Iteration Index is used to enhance the energy efficiency of a UAV system supported by RIS in a (MEC) environment and iterative algorithm is used to optimize the UAV trajectory, bit allocation, and RIS phase shifts. The algorithm consists of three steps, and it is repeated until convergence or until the maximum number of iterations is reached.

10.1 Bit Allocation Optimization:

$$\mathrm{MaX}_{\mathrm{L\,loci}}[\mathrm{n}], \mathrm{LUAVi}[\mathrm{n}] \sum_{n=1}^{N} \mathrm{L}[\mathrm{n}] - \alpha \sum_{n=1}^{N} \mathrm{E}[\mathrm{n}] \tag{16a}$$

$$\text{s.t. } (7e) - (7g) \tag{16b}$$

This step adjusts the local and UAV computation bits l and l UAV to minimize the energy consumption for processing [13]. The gradients represent the partial derivatives of the energy consumption with respect to the computation bits.

10.2 Phase Shift Optimization:

$$Max\ \theta m[n]\ \sum_{n=1}^{N} \sum_{i=1}^{1} BtR_{0ff\pi i}\,[n] \tag{17}$$

Optimizing the phase shifts of the RIS (Reconfigurable Intelligent Surface) improves signal reception and system efficiency [25].

Then, the channel gain between IoTdevice πi[n] and the UAV can be expressed as:

$$\left|\ \mathrm{h}_{\mathrm{U\pi i}}\,[\mathrm{n}] + (\mathrm{h}_{\mathrm{R\pi i})}\,[\mathrm{n}])^{\mathrm{H}} + \mathrm{dig}(\Phi\,[\mathrm{n}])\mathrm{h}_{\mathrm{UR}}\,[\mathrm{n}]\right|^{2} = |h\pi i[n]|\text{^}2 \tag{18}$$

10.3 UAV Trajectory Optimization:

$$Max\ q[n]\ \sum_{n=1}^{N}\sum_{i=1}^{I} \mathrm{BtR}_{0\mathrm{ff\pi i}}\,[\mathrm{n}] - \mathrm{t}\alpha \sum_{n=1}^{N}\left(\mathrm{T1}\,\upsilon^{3}\,[\mathrm{n}] + \frac{\mathrm{T2}}{\upsilon[\mathrm{n}]}\right) \tag{19}$$

This step optimizes the UAV's trajectory to ensure it does not exceed the maximum allowable speed (υ). The gradient represents the change in trajectory required to minimize energy consumption [26] , and packet error rate.

10.4 Algorithm

Algorithm 1 : Energy-Efficient UAV-Assisted IoT Optimization

1. Input: System parameters, initial UAV trajectory, RIS and IoT device positions, phase shifts, and bit allocation.

2. Output: Optimized energy efficiency, bit allocation, phase shifts, and UAV trajectory.

// Initialization

3. Set system parameters.

4. Initialize UAV trajectory, RIS and IoT device positions, phase shifts, bit allocation.

// Solve Optimization Problem

5. Define the objective function and constraints.

6. Calculate the initial values for sensing duration, sensing threshold, UAV transmit power, and packet error rate.

7. While (Energy efficiency change < threshold)

8. Solve Bit Allocation using Gradient Descent: Update local and UAV computation bits using 8.

9. Solve Phase Shift Optimization using Gradient Descent: Update phase shifts of RIS elements using 9.

10. Solve UAV Trajectory Optimization using Gradient Descent: Update UAV trajectory using 11.

11. Update Energy Efficiency based on the updated bit allocation, phase shifts, and UAV trajectory.

12. End

TABLE 2: Simulation Parameters

parameters	*values*
B	*30e6HZ*
Li	*200e6 bits*
M UAV	*0.4kg*
fs	*50e3*
Pt max	*5w*
Pt min	*0.4w*
Ps	*0.2w*
Pc	*0.1w*
I	*6*
H	*40m*
N	*25*
g	*9.8 m/s2*

11. SIMULATION RESULTS

Fig .3 depicts the exact of n on the EE when ps =0.2 w and pt=5w at small n=10 Energy Efficiency is low for rs, moderate increases in improve EE [27] , but excessive increases lead to stabilization without further improvements, affected by distance and time 2%.

Fig. 4 presents the effect of each individual optimization parameter on EE,EE decreases as n increases past a certain point due to excessive Energy consumption for sensing and EE improves with increasing Pt from 0.4 to 5 w initially,but starts to decline after a peak value is reached,increasing packet error rate X drastically reduces EE,highlighting the importance of minimizing data loss.

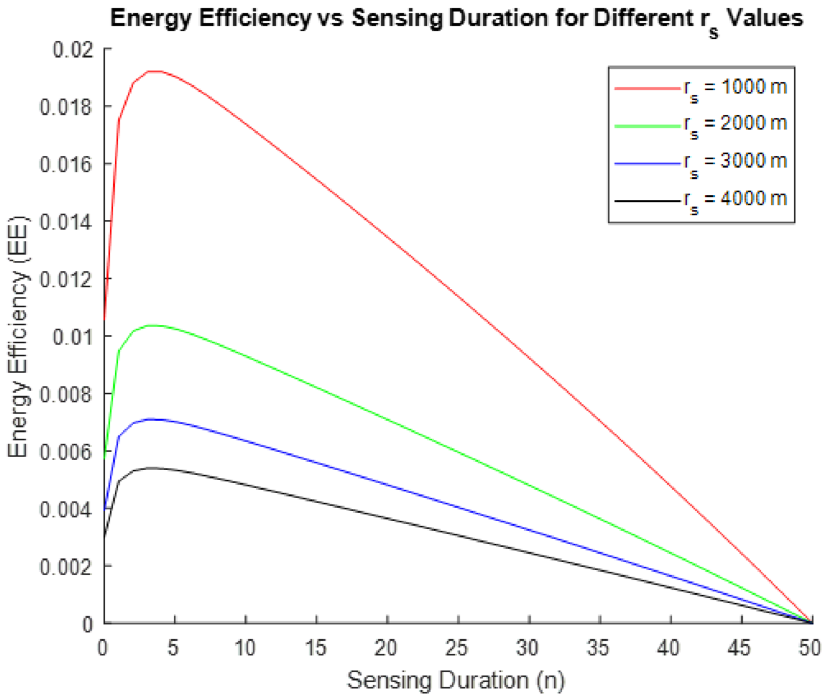

Fig. 3. Energy Efficiency versus the Sensing Duration used (rs=1000,2000,3000 and 4000 m), mUAV=0.4 kg, Nu=4, ru=0.2 m.

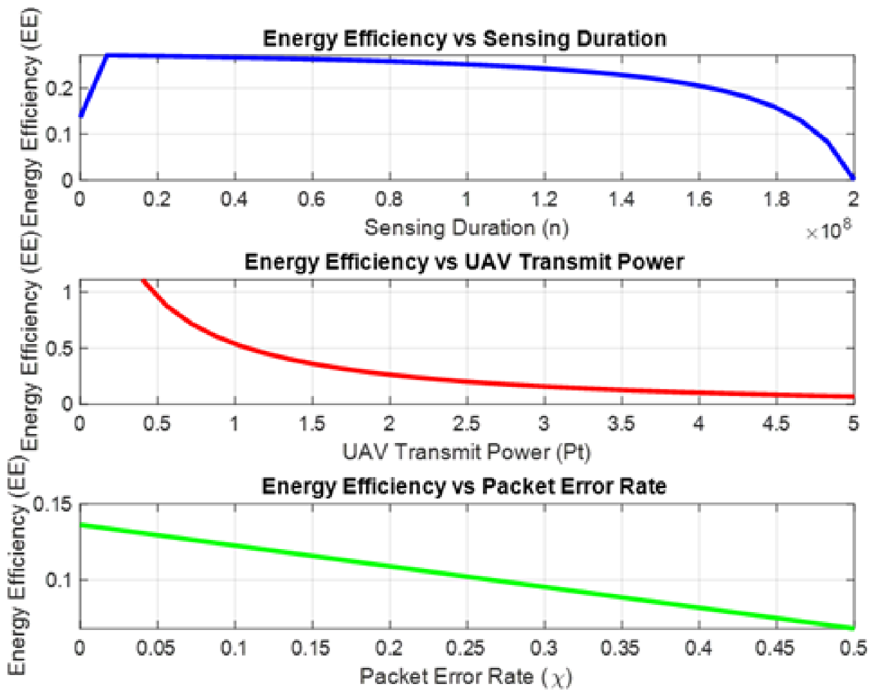

Fig. 4. Energy Efficiency Vs.Each optimization Parameter n=200,fs=50 x103, pc=0.1 ,ps=0.2.

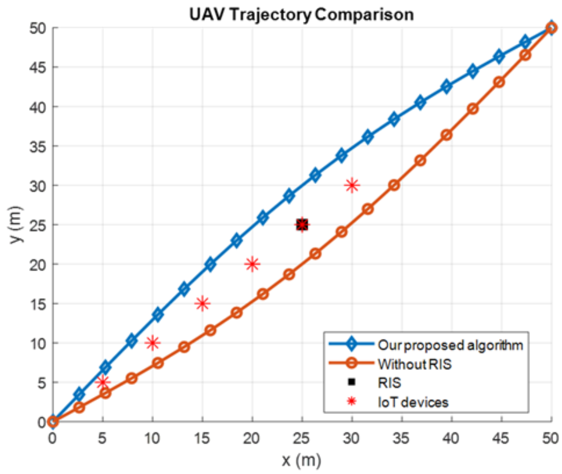

Fig. 5. UAV Trajectories Comparison when H=40m,hR=20m,Vmax=10m/s,N=20.

Fig. 5 depicts the without RIS,the UAV follows a less efficient path,leading to higher power consumption and paths of the UAV 50m and Q0=(0,0),qf=(50,50),wR=(25,25), the RIS position acts as a reflection point, improving communication between the UAV and IOT . IOT Device positions ω1fixed at (5,5),(10,10),(15,15),(20,20),(25,25),(30,30).

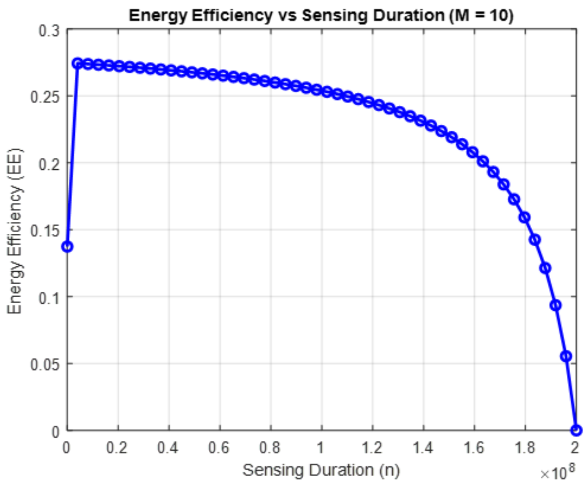

Fig. 6. Energy Efficiency versus.Sensing Duration (M=10)

Fig. 6 However, the EE increased by up to 27% after integration compared to fig 4 before integration of RIS and MEC technologies, which shows a clear effect in increasing EE.n starts from small values and extends to approximately 2x 10^{-8}.

Fig. 7 displays the Due to increased power consumption and computational effort, EE decreases as the number of users increases.

When U=10 to 100, PRIS=10 mW, employing methods such as STAR-RIS increases EE by improving signal quality and lowering power loss. [28]. The most recent research outperforms Studies 1 and 2, improving resource allocation by 5%.

Maximizing EE requires choosing the ideal transmission power [29].Signal enhancement methods, such as RIS, can increase efficiency and lower the requirement for high transmission power.

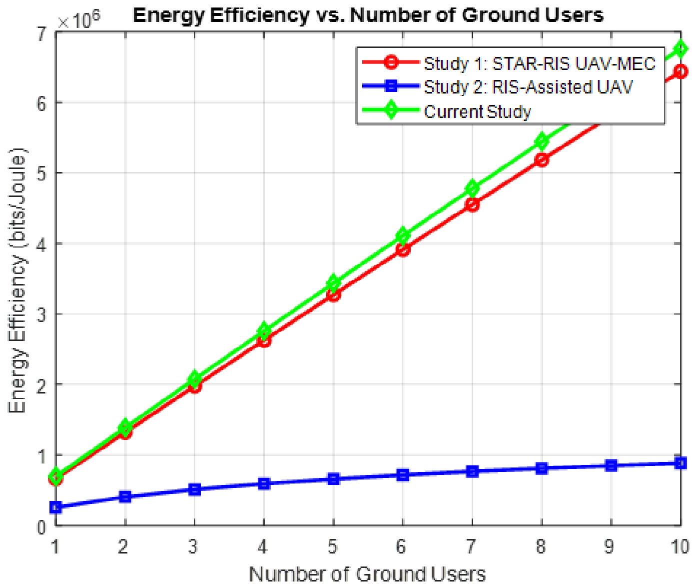

Fig. 7. Energy Efficiency vs. Number of Ground Users S=50Mbps,Pu= o.2 W, N=128, pn=0.01.

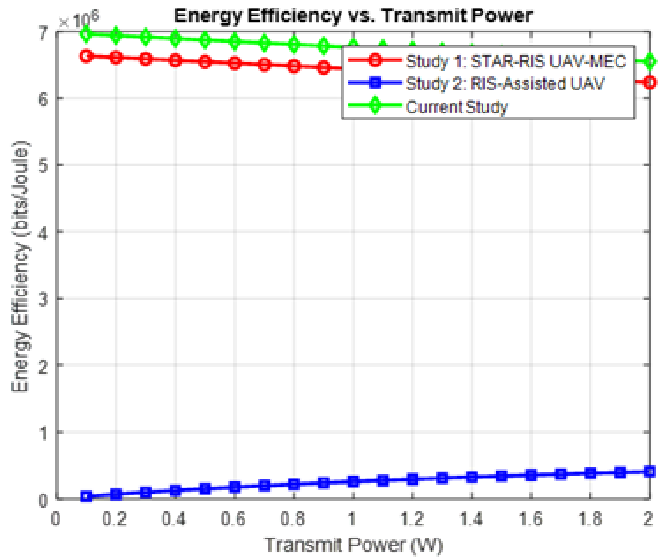

FIGURE 8. Energy Efficiency vs. Transmission Power pRIS =10mW,pt=0.1 to 2 W,PUAV=2 W.

Fig . 8 display the EE is first improved by raising because of increased transmission rates.

12. CONCLUSION

Field tests can check the UAV and RIS system's performance in real-world scenarios, taking into account varied surroundings and UAV models to evaluate parameters such as size and battery capacity. Machine learning can maximize energy efficiency while also supporting multi-objective goals such as increased throughput and reduced latency. Furthermore, scalability can be examined by testing with more IoT devices and researching dynamic network topologies to effectively adapt to changing situations and conditions.

In this study, an integrated system combining UAVs and RIS was created to improve energy efficiency in IoT systems. Significant performance improvements were achieved over conventional systems using an optimization algorithm and gradient descent techniques. The findings indicate that this approach could be extremely useful in future applications where UAVs and RIS are integrated into complex wireless communication systems. These systems can provide broader coverage and higher energy efficiency, making them suitable for a variety of applications such as remote monitoring and communication in remote locations.

REFERENCES

[1] I. Bala, A. Sharma, A. Tselykh, and B.-G. Kim, "Throughput optimization of interference limited cognitive radio-based Internet of Things (CR-IoT) network," J. King Saud Univ. Inf. Sci., vol. 34, no. 7, pp. 4233-4243, 2022. https://doi.org/10.1016/j.jksuci.2022.05.019
[2] R. Prakash and A. Balaji Ganesh, "Internet of Things (IoT) enabled wireless sensor network for physiological data acquisition," in International Conference on Intelligent Computing and Applications, 2019, pp. 163-170. https://doi.org/10.1007/978-981-13-2182-5_17
[3] M. Ghamari, P. Rangel, M. Mehrubeoglu, G. S. Tewolde, and R. S. Sherratt, "Unmanned aerial vehicle communications for civil applications: A review," IEEE Access, vol. 10, pp. 102492-102531, 2022. https://doi.org/10.1109/ACCESS.2022.3208571
[4] M. Dai, N. Huang, Y. Wu, J. Gao, and Z. Su, "Unmanned-aerial-vehicle-assisted wireless networks: Advancements, challenges, and solutions," IEEE Internet Things J., vol. 10, no. 5, pp. 4117-4147, 2022. https://doi.org/10.1109/JIOT.2022.3230786
[5] S. Ashtari Nakhaei, "Knowledge-Defined Routing Strategies for Next Generation Wireless Networks." 2023.
[6] T. M. Hoang, B. C. Nguyen, H. L. T. Thanh, X. N. Tran, and P. T. Hiep, "Finite Block Length NOMA MU Pairing UAV-enable system: Performance Analysis and Optimization," IEEE Trans. Mob. Comput., 2024. https://doi.org/10.1109/TMC.2024.3368159
[7] N. Lin, Y. Fan, L. Zhao, X. Li, and M. Guizani, "GREEN: A global energy efficiency maximization strategy for multi-UAV enabled communication systems," IEEE Trans. Mob. Comput., vol. 22, no. 12, pp. 7104-7120, 2022. https://doi.org/10.1109/TMC.2022.3207791
[8] Y. Zhang et al., "Machine Learning-Based Reliable Transmission for UAV Networks With Hybrid Multiple Access," IEEE Trans. Netw. Serv. Manag., 2024.
[9] M. Ahmed et al., "Active reconfigurable intelligent surfaces: Expanding the frontiers of wireless communication-a survey," IEEE Commun. Surv. Tutorials, 2024. https://doi.org/10.1109/COMST.2024.3423460
[10] A. Narayanan et al., "Key advances in pervasive edge computing for industrial Internet of Things in 5G and beyond," IEEE Access, vol. 8, pp. 206734-206754, 2020. https://doi.org/10.1109/ACCESS.2020.3037717
[11] W. Khalid, M. A. U. Rehman, T. Van Chien, Z. Kaleem, H. Lee, and H. Yu, "Reconfigurable intelligent surface for physical layer security in 6G-IoT: Designs, issues, and advances," IEEE Internet Things J., vol. 11, no. 2, pp. 3599-3613, 2023. https://doi.org/10.1109/JIOT.2023.3297241
[12] G. K. Pandey, D. S. Gurjar, S. Yadav, Y. Jiang, and C. Yuen, "UAV-Assisted Communications With RF Energy Harvesting: A Comprehensive Survey," IEEE Commun. Surv. Tutorials, 2024. https://doi.org/10.1109/COMST.2024.3425597
[13] X. Qin, Z. Song, T. Hou, W. Yu, J. Wang, and X. Sun, "Joint optimization of resource allocation, phase shift, and UAV trajectory for energy-efficient RIS-assisted UAV-enabled MEC systems," IEEE Trans. Green Commun. Netw., vol. 7, no. 4, pp. 1778-1792, 2023. https://doi.org/10.1109/TGCN.2023.3287604

[14] H. Hu, Y. Huang, G. Cheng, Q. Kang, H. Zhang, and Y. Pan, "Optimization of energy efficiency in UAV-enabled cognitive IoT with short packet communication," IEEE Sens. J., vol. 22, no. 12, pp. 12357-12368, 2021. https://doi.org/10.1109/JSEN.2021.3130581

[15] J. Ma, P. Chen, X. Xiong, L. Zhang, S. Yu, and D. Zhang, "Research on Vision-Based Servoing and Trajectory Prediction Strategy for Capturing Illegal Drones," Drones, vol. 8, no. 4, p. 127, 2024. https://doi.org/10.3390/drones8040127

[16] E. Trigui, M. Esseghir, and L. Merghem-Boulahia, "Multi-agent systems negotiation approach for handoff in mobile cognitive radio networks," in 2012 5th International Conference on New Technologies, Mobility and Security (NTMS), 2012, pp. 1-5. https://doi.org/10.1109/NTMS.2012.6208687

[17] X. Qin, W. Yu, Z. Song, T. Hou, Y. Hao, and X. Sun, "Energy efficiency optimization for RIS-assisted UAV-enabled MEC systems," in 2022 IEEE Globecom Workshops (GC Wkshps), 2022, pp. 1164-1169. https://doi.org/10.1109/GCWkshps56602.2022.10008478

[18] N. Crespi, W. Nagmeldin, and A. Abdelmaboud, "Vehicles Base Stations for Ad Hoc Networks," pp. 1-16, 2022.

[19] A. S. Parihar, K. Singh, V. Bhatia, C.-P. Li, and T. Q. Duong, "Performance Analysis of NOMA Enabled Active RIS-Aided MIMO Heterogeneous IoT Networks With Integrated Sensing and Communication," IEEE Internet Things J., 2024. https://doi.org/10.1109/JIOT.2024.3416951

[20] M. Diamanti, M. Tsampazi, E. E. Tsiropoulou, and S. Papavassiliou, "Energy efficient multi-user communications aided by reconfigurable intelligent surfaces and UAVs," in 2021 IEEE International Conference on Smart Computing (SMARTCOMP), 2021, pp. 371-376. https://doi.org/10.1109/SMARTCOMP52413.2021.00075

[21] K. Lee, "Low-complexity transmit power control for secure communications in wireless-powered cognitive radio networks," Sensors, vol. 21, no. 23, 2021. https://doi.org/10.3390/s21237837

[22] G. M. D. Santana, R. S. de Cristo, and K. R. L. J. C. Branco, "Integrating cognitive radio with unmanned aerial vehicles: An overview," Sensors (Switzerland), vol. 21, no. 3, pp. 1-27, 2021. https://doi.org/10.3390/s21030830

[23] A. Kumar, H. M. Alshahrani, F. Alotaibi, and A. Nanthaamornphong, "A hybrid detection algorithm for 5G OTFS waveform for 64 and 256 QAM with Rayleigh and Rician channels," Open Eng., vol. 14, no. 1, p. 20240008, 2024. https://doi.org/10.1515/eng-2024-0008

[24] M. Abrar, U. Ajmal, Z. M. Almohaimeed, X. Gui, R. Akram, and R. Masroor, "Energy efficient UAV-enabled mobile edge computing for IoT devices: A review," IEEE Access, vol. 9, pp. 127779-127798, 2021. https://doi.org/10.1109/ACCESS.2021.3112104

[25] S. Abeywickrama, R. Zhang, Q. Wu, and C. Yuen, "Intelligent reflecting surface: Practical phase shift model and beamforming optimization," IEEE Trans. Commun., vol. 68, no. 9, pp. 5849-5863, 2020. https://doi.org/10.1109/TCOMM.2020.3001125

[26] J. Won, D.-Y. Kim, Y.-I. Park, and J.-W. Lee, "A survey on UAV placement and trajectory optimization in communication networks: From the perspective of air-to-ground channel models," ICT Express, vol. 9, no. 3, pp. 385-397, 2023. https://doi.org/10.1016/j.icte.2022.01.015

[27] H. Hu, Y. Huang, G. Cheng, Q. Kang, H. Zhang, and Y. Pan, "Optimization of Energy Efficiency in UAV-Enabled Cognitive IoT with Short Packet Communication," IEEE Sens. J., vol. 22, no. 12, pp. 12357-12368, 2022, doi: 10.1109/JSEN.2021.3130581. https://doi.org/10.1109/JSEN.2021.3130581

[28] M. S. Al-abiad, "Energy Efficient Communications in RIS-assisted UAV Networks Based on Genetic Algorithm".

[29] H. Xiao, S. Member, and X. Hu, "Energy-Efficient STAR-RIS Enhanced UAV-Enabled MEC Networks with Bi-Directional Task Offloading," pp. 1-14.

ASIAN JOURNAL OF ELECTRICAL AND ELECTRONIC ENGINEERING
Vol. 5 No. 1 2025
E-ISSN: 2785-8189

Performance Analysis of a Microcontroller-Based Overvoltage and Overcurrent Protection System

Mohammad Iftekher Uddin[1], Muhammad Mahbubur Rashid [2], and S M Salam[2*]

[1]*Dept. of EEE, CUET, Chattogram, Bangladesh*
[2]*Dept. of Mechatronics Engineering, International Islamic University Malaysia, Kuala Lumpur, Malaysia*

*Corresponding: s.munimus@live.iium.edu.my

(Received: 24 June 2025; Accepted: 21 July 2025)

Abstract— A microcontroller-based over-voltage and over-current monitoring and protection systems have been developed to enhance the safety and reliability of electrical systems by automatically disconnecting the circuit under fault conditions. The system integrates a PIC18F2550 microcontroller, relay switches, transistors, current transformers (CT), potential transformers (PT), and other discrete components, with a Windows-based graphical user interface (GUI) programmed in Visual Basic and USB communication for real-time monitoring and control. The microcontroller processes voltage and current signals from the CT and PT, compares them against predefined threshold values, and activates the relay driver through a transistor when an over-voltage or over-current condition is detected, disconnecting the circuit after a brief delay to prevent damage. Experimental results validate the system's effectiveness; for example, it successfully triggered protection at 4.7 A against a 4.5 A current threshold and at 214 V against a 210 V voltage threshold. Various test scenarios confirmed the system's reliability in identifying and responding to faulty conditions. Compared to recent research, the proposed design demonstrates improved performance in detection speed, operational accuracy, and system simplicity, offering a robust and cost-effective solution for modern electrical protection needs.

Keywords: *Microcontroller, Static Relay, Fault protection*

1. INTRODUCTION

Electrical systems are often exposed to risks from voltage and current fluctuations, which can result in equipment failure, reduced operational lifespan, or even fire hazards. An effective protection mechanism is essential, particularly in industrial and residential setups where reliability is crucial. This work focuses on developing a microcontroller-based system that continuously monitors voltage and current, compares them with predefined safe limits, and triggers protection mechanisms when thresholds are exceeded.

Monitoring and controlling over-voltage and over-current conditions in power systems are crucial for maintaining the integrity and reliability of electrical infrastructure [1]. Electrical components such as transformers, insulators, generators, and transmission lines are susceptible to damage when subjected to electrical parameters exceeding their normal operating ranges. These anomalies can result from various factors, including consumer negligence, circuit breaker operations, lightning strikes, and grounding faults. Implementing effective protection mechanisms is essential to prevent equipment damage, ensure operational continuity, and enhance safety [2]. Traditional protection systems often rely on electromechanical relays and analog circuits, which, while effective, may lack the flexibility and precision required for modern applications [3]. The advent of microcontroller-based solutions offers a more adaptable and cost-effective approach to protection systems. Microcontrollers enable precise monitoring and control, facilitating real-time response to fault conditions and integration with user interfaces for enhanced system interaction [4].

In recent years, several studies have explored microcontroller-based protection systems. For instance, a study presented the design and implementation of an Arduino-based under-voltage and over-voltage protection system, utilizing components such as voltage regulators, bridge rectifiers, step-down transformers, relay modules, and

DOI: https://doi.org/10.69955/ajoeee.2025.v5i1.77

LCD displays to monitor and protect against voltage fluctuations [5]. Another research focused on a low-cost under- and over-voltage protective device fabricated using a microcontroller, transistors, ICs, and other discrete components, aiming to provide reliable protection for home and office appliances [6][7]. Additionally, a microcontroller-based over-voltage and under-voltage protection circuit was developed using an Arduino Nano to monitor voltage and control a relay for isolating loads during abnormal voltage conditions [8][9].

Building on previous advancements, this work introduces a microcontroller-based system for monitoring and protecting against over-voltage and over-current conditions. The system features a Windows-based graphical user interface (GUI) developed in Visual Basic, providing an intuitive platform for real-time interaction. The microcontroller processes input signals from the CT and PT, evaluates them against predefined thresholds, and controls relay drivers via transistors [10]. When fault conditions are detected, the system triggers a brief delay before disconnecting the circuit to mitigate potential damage. Experimental validation confirms the system's efficiency in real-time monitoring and its reliability in protecting electrical systems from faults. In summary, the proposed design offers a robust solution for protecting electrical systems from over-voltage and over-current conditions, enhancing safety and reliability through precise monitoring and control facilitated by microcontroller technology.

2. DESIGN AND METHODOLOGY

The design of the microcontroller-based over-voltage and over-current monitoring and protection system revolves around real-time sensing, intelligent decision-making, and automatic circuit isolation. The core of the system is a PIC18F4550 microcontroller, which interfaces with both voltage and current sensing modules to monitor the electrical conditions of a three-phase power system. These sensors detect anomalies such as voltage spikes or excessive current draw, converting analog signals into digital values through a rectifier and feeding them into the microcontroller's ADC inputs. A user interface allows operators to set threshold values and observe real-time readings, while the microcontroller continuously compares incoming data against these limits.

The methodology involves three primary stages: sensing, processing, and protection. First, AC voltage and current sensors capture the electrical parameters, which are rectified and filtered to ensure signal stability. The microcontroller processes these values in real-time, using predefined logic to determine if the parameters exceed safe operational boundaries. If a fault is detected, the system immediately activates driver circuits connected to relays, disconnecting the affected phase to protect the load. This is done independently for each of the three phases to ensure targeted protection. Additionally, the system can display alerts, store fault data, and reset once conditions normalize, making it highly efficient, responsive, and suitable for industrial or residential electrical safety applications.

2.1 Formulation of block diagram

The diagram illustrates a microcontroller-based system designed for over-voltage and over-current monitoring and protection in a three-phase electrical network. Central to the system is the PIC18F4550 microcontroller, which receives analog inputs from both AC voltage and current sensing modules. These sensed signals are first rectified to convert them into a suitable DC level for processing by the microcontroller's ADC inputs. The microcontroller continuously analyzes these inputs and checks them against predefined safety thresholds to detect any abnormal electrical conditions.

When an over-voltage or over-current is identified in any of the three phases, the microcontroller sends control signals to dedicated driver circuits corresponding to Phase 1, Phase 2, and Phase 3, thereby disconnecting the affected phase from the load to prevent damage. The system includes a user interface, allowing users to view real-time voltage and current values, adjust protection thresholds, and reset the system if needed. This modular and real-time monitoring approach enhances the safety, efficiency, and reliability of the power distribution system, making it suitable for both industrial and residential applications.

The microcontroller-based over-voltage and over-current monitoring and protection system is designed to provide efficient fault detection and protection by integrating hardware and software components.

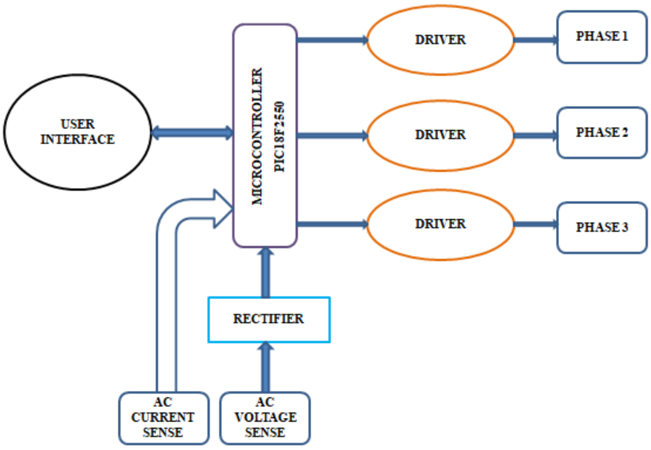

Fig. 1. *Block diagram of the system*.

2.2 *System Operation and Result*

The proposed microcontroller-based over-voltage and over-current protection system has been carefully designed and implemented to ensure reliable monitoring and safeguard against electrical faults in a three-phase power supply environment. The hardware design is centered around the PIC18F2550 microcontroller, which receives voltage and current inputs through Potential Transformers (PTs) and Current Transformers (CTs). These inputs are scaled and filtered before being processed by the microcontroller's ADC channels. The system also incorporates relay switches and transistor-based drivers for each phase, allowing the microcontroller to isolate faulty phases based on measured electrical parameters. A USB interface enables seamless communication with a Windows-based GUI, which facilitates real-time monitoring and user interaction.

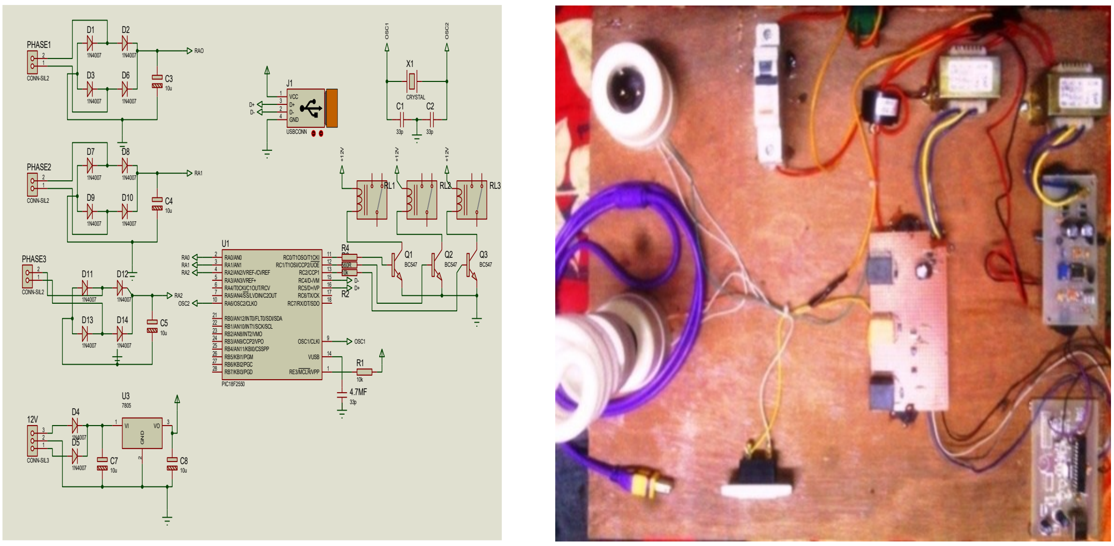

(a) (b)

Fig. 2. *Circuit diagram of the system*

The software component includes embedded C programming for the microcontroller and a Visual Basic-based GUI for the user interface. The microcontroller is programmed to constantly evaluate the analog voltage and current inputs, compare them to user-defined thresholds, and trigger relay operations if fault conditions are detected. A delay logic is embedded in the code to prevent false tripping due to temporary surges or noise. The GUI allows users to view real-time system behavior, adjust threshold parameters, and receive alerts when faults occur, ensuring a user-friendly yet robust interaction framework.

Figures 2 (a) and (b) provide a clear visualization of the system's implementation. Figure 2 (a) shows the full circuit diagram, which includes three sets of relays, transistors, and driver circuits corresponding to each of the three phases. The rectifier circuit converts the sensed AC signals into DC voltages suitable for microcontroller processing. Figure 2 (b) presents the snapshot of the actual built system, showcasing the physical integration of components such as the microcontroller board, sensing elements, and relays. These diagrams are essential in demonstrating both the theoretical design and the practical realization of the system.

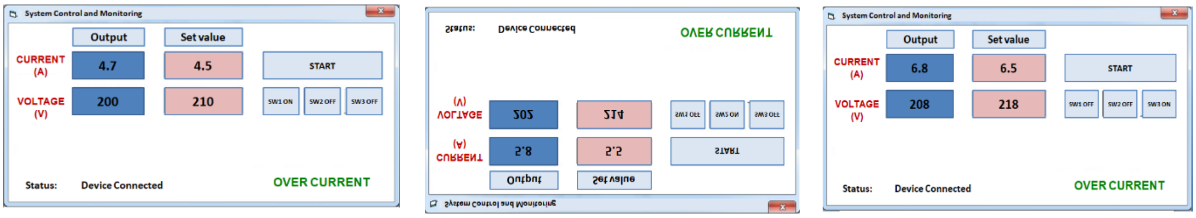

(a) (b) (c)

Fig 3. Monitor and protect the system with different over current conditions.

The system's performance was tested against several over-current conditions, as illustrated in Figures 3 a, b, and c and finally summarized in Table 1. Each figure shows the system in operation under different threshold settings. For example, in Figure 4, the threshold voltage is set to 210V, and the current threshold is 4.5A. The output current measured was 4.7A, slightly exceeding the threshold, which activated Switch 1 to protect the system. Similarly, Figures 3(a) and 3(b) show higher thresholds and corresponding over-current conditions with Switch 2 activated. Table 1 compiles this data, confirming the relay response in each scenario and validating the system's reliability in managing over-current events.

Table 1: Summary table of over-current faults based on the data provided.

Figure	Threshold Current (A)	Threshold Voltage (V)	Switch State	Output Current (A)	Over-Current Condition
3(a)	4.5	210	Switch 1 ON	4.7	Yes
3(b)	5.5	214	Switch 2 ON	5.8	Yes
3(c)	6.5	218	Switch 2 ON	6.8	Yes

The over-voltage protection functionality is demonstrated in Figures 4 a, b, and c is summarized in Table 2. In these tests, the output voltage surpassed the predefined threshold levels despite varying current conditions. For instance, Figure 4(a) shows an output voltage of 214V against a threshold of 210V, causing Switch 1 to engage.

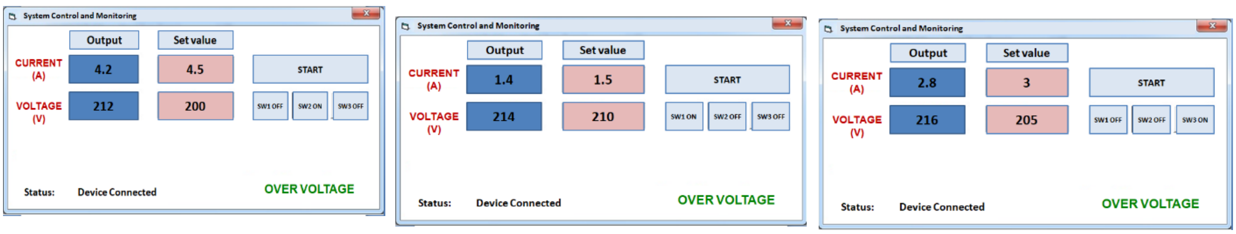

(a) (b) (c)

Fig 4. Monitor and protect the system with different over voltage conditions.

Likewise, Figures 4(b) and 4(c) display over-voltage responses at lower current levels, activating Switch 2 and Switch 3, respectively. Table 2 details each condition, emphasizing the system's ability to respond accurately across varying voltages and current combinations. This confirms that the protection system reliably detects and mitigates both over-current and over-voltage faults, thereby enhancing electrical safety in practical applications.

Table 2: Summary table of over-voltage faults based on the provided data.

Figure	Threshold Current (A)	Threshold Voltage (V)	Switch State	Output Voltage (V)	Over-Voltage Condition
4(a)	1.5	210	Switch 1 ON	214	Yes
4(b)	4.5	200	Switch 2 ON	212	Yes
4(c)	3	205	Switch 3 ON	216	Yes

2.3 Comparison of performance

Compared to the system presented by [11], which utilizes an Arduino Uno without GUI interface and has a response time of 250 ms, our proposed model achieves faster response (~200 ms) and supports three-phase operation with USB-based GUI for real-time control. Additionally, the error margin of ±1.5% is lower than those reported by, indicating higher reliability in fault detection. Another paper [12], which also used Using Relay Module and Python-Based Algorithm.

Table 3: A **comparison table** with similar research

Feature / Metric	***System (PIC18F2550)***	***Paper [11] (STM32)***	***Paper [12] (Arduino Uno)***
Voltage Threshold Range	*200–220 V*	*180–250 V*	*190–230 V*
Current Threshold Range	*1.5–6.5 A*	*0.5–10 A*	*2–7 A*
Response Time	*~200 ms*	*150 ms*	*250 ms*
Error Rate / Tolerance	*±1.5%*	*±2%*	*±3%*
Relay Activation Method	*Transistor + Relay*	*Solid-state relay*	*Mechanical relay*
GUI Availability	*Yes (Visual Basic)*	*No*	*Yes (Python Tkinter)*

The comparative analysis of the microcontroller-based over-voltage and over-current protection system using the PIC18F2550 with systems from Paper [11] (STM32-based) and Paper [12] (Arduino Uno-based) highlights notable strengths and trade-offs. The proposed system offers a balanced and efficient design, particularly with its voltage threshold range of 200 – 220 V and current threshold detection between 1.5 – 6.5 A, suitable for mid-range residential and industrial applications. While the STM32-based system in Paper [11] supports a wider range (180 – 250 V, 0.5 – 10 A), and the Arduino-based system in Paper [12] accommodates slightly higher current (up to 7 A), the PIC-based design delivers a reliable middle ground, maintaining precision without complexity.

In terms of response time and accuracy, the STM32 system leads with a faster 150 ms response, yet the

PIC18F2550 design maintains competitive performance at approximately 200 ms and outperforms the Arduino Uno system, which responds in 250 ms. Most notably, the PIC system achieves a lower error rate (±1.5%) compared to STM32 (±2%) and Arduino Uno (±3%), indicating higher reliability in real-time fault detection. Furthermore, the PIC18F2550 system includes a fully functional Visual Basic-based GUI for real-time monitoring and control—something absents in the STM32 model and only partially implemented in the Arduino design. The use of transistor-driven relays enhances circuit protection and switching precision, compared to mechanical relays in Paper [12] and solid-state relays in Paper [11]. This comparison underscores the strength of the PIC-based system in balancing performance, reliability, and usability, making it a cost-effective and dependable solution for fault monitoring and protection.

3. CONCLUSION

This paper presents a straightforward and effective approach to mitigating over-voltage and over-current conditions using a microcontroller-based system. The proposed system integrates a PIC18F2550 microcontroller, current and potential transformers (CT and PT), relay switches, and a user-friendly GUI programmed in Visual Basic for real-time monitoring and control. The microcontroller continuously evaluates load voltage and current against predefined threshold values. If these parameters remain within acceptable limits, the relay maintains the circuit, allowing uninterrupted current flow to the load. However, when voltage or current surpasses the preset thresholds due to faults, the system promptly activates the relay to isolate the load from the supply, thereby preventing potential damage. Experimental findings validate the system's reliability and efficiency. For example, at a threshold current of 5.5A and a voltage of 214V, the system successfully detected an over-current condition at 5.8A and an over-voltage condition at 212V, promptly triggering the protection mechanism. The integration of a GUI enhances user interaction and monitoring capabilities, offering a comprehensive solution for managing fault conditions. This system demonstrates a robust and cost-effective method to safeguard electrical systems, providing enhanced reliability for protecting home and office appliances from electrical faults. The design's simplicity and effectiveness make it a valuable contribution to modern electrical protection technologies.

REFERENCES

[1] H. Rezaie and M. H. Kazemi-Rahbar, "Enhancing voltage stability and LVRT capability of a wind-integrated power system using a fuzzy-based SVC," Engineering Science and Technology, an International Journal, vol. 22, no. 3, pp. 827-839, 2019. https://doi.org/10.1016/j.jestch.2018.12.018

[2] S. Aslam, A. Altaweel, and A. B. Nassif, "Optimization Algorithms in Smart Grids: A Systematic Literature Review," 2023, [Online]. Available: http://arxiv.org/abs/2301.07512

[3] S. M. Salam, N. Mohammad, and F. Hossain, "A new approach to Analysis the Impact of Demand Side Management for Temperature Control Load Consideration in a Test Bus System," 2021 5th International Conference on Electrical Information and Communication Technology, EICT 2021, 2021.https://doi.org/10.1109/EICT54103.2021.9733717

[4] K. Majumdar, P. K. Roy, and S. Banerjee, "Framework of hybrid renewable energy with conventional power generation scheduling using novel metaheuristic optimization algorithm," International Journal of Power and Energy Systems, vol. 42, no. 10, 2022. https://doi.org/10.2316/J.2022.203-0387

[5] M. M. Rashid, S. M. Salam, M. Y. Ali, and S. Yvette, "Flywheel energy storage for peak shaving and load balancing in power grids," in proceedings of 5th international conference on sustainable innovation in engineering and technology 2023, AIP publishing, Aug. 2024, p. 020127. https://doi.org/10.1063/5.0229871

[6] B. F. W. Allen J. Wood, Power Generation, Operation, and Control . John Wiley & Sons, Inc, 1996.

[7] S. M. Salam and N. Mohammad, "Analyze the Impact of Demand Side Management on Grid Power for an Isolate Zone in a Sustainable IEEE 14 Bus System," in 2021 International Conference on Information and Communication Technology for Sustainable Development, ICICT4SD 2021 - Proceedings, 2021, pp. 16-20. https://doi.org/10.1109/ICICT4SD50815.2021.9396975
[8] C. Brusil, H. Arcos, F. Espín and C. Velásquez, "Analysis of Harmonic Distortion of LED Luminaires Connected to Utility Grid," 2020 IEEE ANDESCON, Quito, Ecuador, 2020, pp. 1-6. https://doi.org/10.1109/ANDESCON50619.2020.9272004
[9] A. Powers and M. Saad, "Building Energy Use: Modeling and Analysis of Lighting Systems-A Case Study," Sustainability, vol. 14, no. 20, p. 13181, Oct. 2022. https://doi.org/10.3390/su142013181
[10] S. M. Salam, M. M. Rashid, M. Y. Ali, and S. Yvette, "Performance analysis of an efficient buck boost converter," AIP Conference Proceedings, 2024, Vol. 3161, No. 1, p. 020128. https://doi.org/10.1063/5.0229872
[11] O. S. Alegu, M. Ezike, D. A. Amoke, and C. Ogbuka, "Design and Construction of a Microcontroller-Based Overcurrent Protection Scheme for Power Transformers With IOT Interface," 2025.
[12] R. Masood Larik, S. Aqeel Haider, K. Attaullah Balochistan, and A. Amjad, "Over-Voltage Protection Circuit for Tripping & Switching of 220V Appliances Using Relay Module," 2025. [Online]. Available: https://www.researchgate.net/publication/390494867

ASIAN JOURNAL OF ELECTRICAL AND ELECTRONIC ENGINEERING
Vol. 5 No. 1 2025
E-ISSN: 2785-8189

Design and Analysis of Digital Control Buck Converter for optimum performance

Nur Ain Elisa Razali*, and A.H.M Zahirul Alam

Dept of Electrical and Computer Engineering, International Islamic University Malaysia, Kuala Lumpur, Malaysia

*Corresponding author: rzalielisa@gmail.com

(Received: 3 July 2025; Accepted: 16 July 2025)

Abstract— This paper aims to design and analyze a digitally controlled buck converter meant for applications requiring DC voltage under varying input voltages and load conditions. The buck converter is designed with a switching frequency of 40 kHz, an inductor value of 200 µH, and a capacitor of 100 µF with Pulse Width Modulation (PWM). The Proportional-Integral (PI) controller is used to maintain the output voltage steady. For simulation and performance evaluation, PSpice and MATLAB/Simulink software are selected. This paper aims to create a digital control system that is better than the traditional analog controllers, offering precise and adaptive regulation. The simulation results highlight how effective the digital PI controller is at reducing voltage ripple and maintaining the output voltage, even when the inputs and loads vary. This study covers detailed parameter calculations, controller design, circuit simulation, and performance analysis, providing a thorough overview of the digitally controlled buck converter system.

Keywords: *Buck Converter, MATLAB, PSpice, Pulse Width Modulation (PWM), and PI controller*

1. INTRODUCTION

The modern electronic devices rely heavily on having a consistent supply voltage, which is where voltage regulators come into play. Among these, DC-DC converters are essential in power electronics, converting an unregulated DC input into a regulated DC output using various techniques. The ability to efficiently manage power between different voltage levels is crucial in applications ranging from consumer electronics to industrial systems [1].

One of the standout topologies in this realm is the buck converter, often referred to as a step-down DC-DC converter. Buck converters are prized for their efficiency, compact size, and their ability to fit into battery-powered and space-limited applications. The increasing demand for higher efficiency and miniaturization in electronic devices has propelled the global DC-DC converter market, making research in this field more important than ever[2].

To boost the performance of buck converters, it's crucial to implement advanced control mechanisms. The Proportional Integral (PI) controller is famous as it effectively reduces the voltage output fluctuation and enhances the transient response [2]. PI controllers help by responding more swiftly to load changes and achieving better overall stability. Despite widespread use, buck converters still face a number of ongoing challenges. Some of the main issues include energy loss, voltage instability, difficulties with thermal management, and electromagnetic interference (EMI), which can affect performance and reliability [3].

Traditional analog control circuits often find it tough to maintain high performance when input voltages vary and load conditions change. The output voltage's sensitivity to duty-cycle variations calls for strong control strategies to ensure stable operation, particularly when input conditions are inconsistent. This paper presents to design of a buck converter suitable for general-purpose DC voltage regulation in both low-power and high-power

DOI: https://doi.org/10.69955/ajoeee.2025.v1i1.74

systems, to develop a digital control system for the designed buck converter, and to analyze the performance of the buck converter equipped with this digital control system.

Previous researchers have mentioned various control strategies for buck converters, such as Proportional-Integral (PI) controllers [2], Sliding Mode Control (SMC) [4], and Fuzzy Logic control [1]. Yet, these methods often face limitations in dynamic environments or require complicated analog circuitry. This study offers a solution by implementing a digital control system that utilizes PWM and PI control theories, aiming to reduce peak currents during transients and improve both reliability and efficiency [2]. The approach builds upon and extends the findings of prior works, offering a digitally controlled buck converter with broad applicability and optimized performance for contemporary electronic systems

2. DESIGN OF CONVERTER

The methodology includes calculating essential parameters, choosing the right components, developing a digital control system, and running thorough simulations using MATLAB/Simulink and PSpice. The entire process is organized to ensure that it can be simulated and the performance can be analyzed under different conditions.

2.1 Buck Converter System

2.1.1. Design Specifications

The converter is designed to reduce a 24V DC input down to a stable 6V DC output, making it suitable for various low- and high-power applications. A switching frequency of 40 kHz has been chosen to strike a balance between efficiency and component size while minimizing output voltage ripple. To find the required duty cycle, D, the standard buck converter is in Eqn (1),

$$D = \frac{V_{OUT}}{V_{IN}} \tag{1}$$

Next, determine the inductor value (L) to keep the inductor current ripple within 10% of the maximum load current, as shown in Eq. (2) is determined. The calculated value for L is 93.75 μH.

$$L = \frac{V_g\,(1-D)\,D \times \frac{1}{f_S}}{\Delta I_L \times 2} \tag{2}$$

The ripple current and voltage must stay below the maximum specification limit of the capacitor [5]. The output capacitor (C) is selected to keep the output voltage ripple to just 1% of V_{out} as indicated in Eq. (3).

$$C = \frac{\Delta I_L}{(\Delta V_{OUT} \times f_S \times 8)} \tag{3}$$

MOSFET is chosen for its quick switching capabilities and low on-resistance as the switch, a Schottky diode for its low forward voltage drop and high switching speed [6], and a load resistance that varies from 1Ω to 1kΩ during simulations to evaluate the circuit's robustness.

2.1.2. Controller Design

To get the precise output voltage, Pulse Width Modulation (PWM) is important in controlling the switching of the MOSFET. In this project, a PI controller is used to tune the PWM signal by adjusting the duty cycle, D, to reduce the steady-state error and enhance the transient response.

2.2 Simulation and Analysis

2.2.1 Simulation Tools

PSpice is used to design a detailed circuit, validate the switching behavior, and analyze the component interaction. MATLAB/Simulink, on the other hand, is important when designing the PI controller and analyzing the results.

2.2.2 Circuit Design and Control Logic

The converter circuit is built in PSpice and also MATLAB/Simulink, integrating the calculated values for inductance (L) and capacitance (C), along with the MOSFET switch, Schottky diode, and a variable load. The PWM and PI controllers are implemented using MATLAB/Simulink, where feedback from the output voltage is used to dynamically adjust the PWM duty cycle. To ensure the simulation runs optimally, various combinations of inductance and capacitance are tested. Table 2.1 summarizes the results, with L set at 200 µH and C at 100 µF chosen for the final MATLAB model due to their excellent transient and steady-state characteristics.

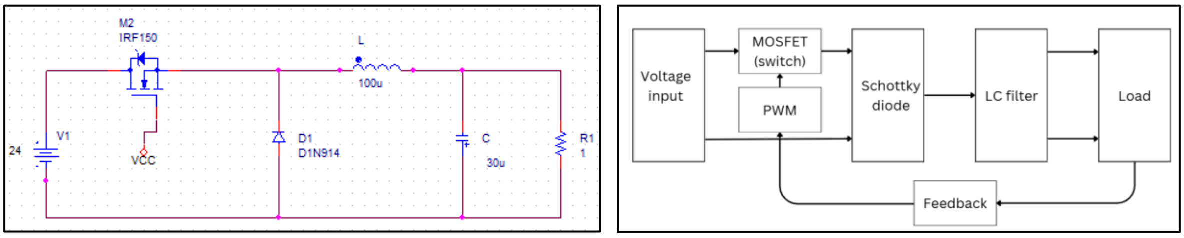

a) b)

Fig 1. a) Schematic diagram for the buck converter, b) detailed Internal Block Diagram of a Buck Converter

2.2.3 Parameter Optimisation

To ensure optimal performance in simulation, various combinations of inductance and capacitance are tested. Table 3.1 summarises the results, with L = 200 µH and C = 100 µF selected for the final MATLAB model due to their superior transient and steady-state characteristics.

Table. 1 Design parameters C and L, and the output responses for different values of C and L

L (µH)	C (µF)	$\Delta I_L\ (A)$ (< 0.6)	$I_L\ (peak)(A)$	$I_L\ (rms)$	I_{CIN}	ESR	$\Delta V_{out}(V)$ (< 0.06)
100	30	1.125	6.5625	6.0088	2.2733	- 0.0508	0.0600
150	30	0.750	6.375	6.0039	2.2604	- 0.0242	0.0599
200	30	0.5625	6.2813	6.0022	2.2559	0.0025	0.06
200	68	0.5625	6.2813	6.0022	2.2559	0.0607	0.0599
200	100	0.5625	6.2813	6.0022	2.2559	0.0754	0.0599

2.2.4 Simulation Configuration

The solver type is carefully chosen to accurately model the fast-switching events and dynamic response of the control system. Additionally, the sampling frequency is set equal to the switching frequency of 40 kHz to enable precise emulation of the digital control signals and maintain synchronization with the MOSFET switching.

2.2.4 Execution and Data Analysis

Simulation has been done to observe and record the stability of the output voltage and ripple, as well as the waveforms of the inductor current. The system responds to sudden changes in load resistance, ranging from 1Ω to 1kΩ, to assess its robustness. The results from these simulations help to validate the initial design.

3. RESULTS AND DISCUSSION

The results are based on the PSpice and MATLAB/Simulink by showing how the converter behaves under a variety of ideal and non-ideal conditions, such as changes in load resistance, capacitance, inductance, duty cycle, and input voltage, along with the effects of parasitic resistances and diode forward voltage drops.

3.1 PSpice Simulations

PSpice simulations using practical approximations for the calculated inductor L = 100 µH and capacitor C = 30 µF values have been carried out. These simulations were designed to help understand how the buck converter performs across different operating conditions.

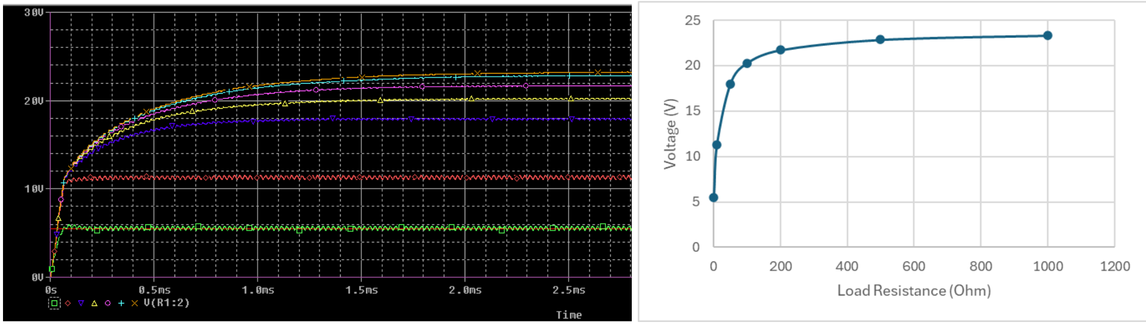

a) b)

Fig. 3. Sweep Analysis with Varying Load in a) PSpice, b) Excel

Figure 3 shows that as the load resistance increased from 1Ω to 1 kΩ, the output voltage also increased because a higher load resistance draws less current from the converter. Thus, reduces voltage drops across internal components like the inductor's resistance and the switch. This highlights the importance of having a controller to keep the output voltage stable, even with different loads.

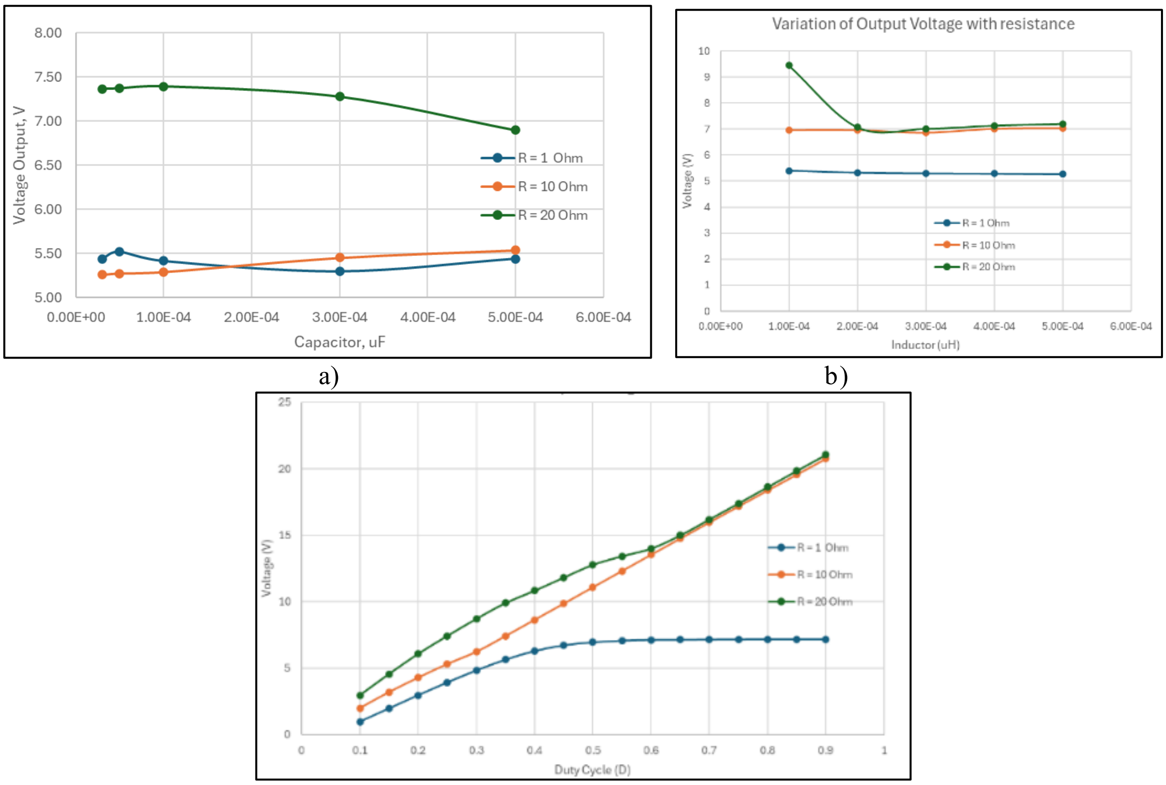

a) b)

c)

Fig. 4 Output voltage variation with the variation of (a) Capacitance, (b) Inductance, and (c) Duty cycle

Figure 4 shows the results for voltage output by varying the capacitance, inductance, and also the duty cycle in the PSpice.

The Fig. 4 (a) shows the capacitance from 30 µF to 500 µF with L=100 µH. The results show that higher capacitance increases the output voltage stability by reducing ripple. A bigger capacitor does a better job of holding the voltage steady during those switching and load changes.

The Fig. 4 (b) shows the inductance value ranging from 100 µH to 500 µH with C= 30 µF. The output voltage stability improved, and the current ripple was reduced, especially for low-resistance loads. Even with lower loads, the higher inductance delivered a smoother output, although the effects weren't as dramatic.

Fig. 4 (c) shows that the output voltage increases with the duty cycle, which aligns with an ideal buck converter. However, at lower resistances like 0.1 Ω, the higher current led to increased losses in the switch, inductor, and wiring. This caused noticeable deviations from the ideal output, highlighting the importance of considering real-world losses in the design. In this design, the lowest resistance value that the PI controller can manage is 0.1 Ω, while the highest is 2 kΩ.

3.2 MATLAB Simulations

The MATLAB/Simulink was used, which included implementing a Proportional-Integral (PI) controller to regulate the output voltage, and the block diagram is shown in Fig. 5. The best L and C values for our MATLAB simulations are 200 µH and 100 µF, respectively, as they struck a great balance between low current ripple and minimal output voltage ripple.

3.2.1 Ideal Case

In the ideal case, simulations were performed without accounting for real-world losses or imperfections.

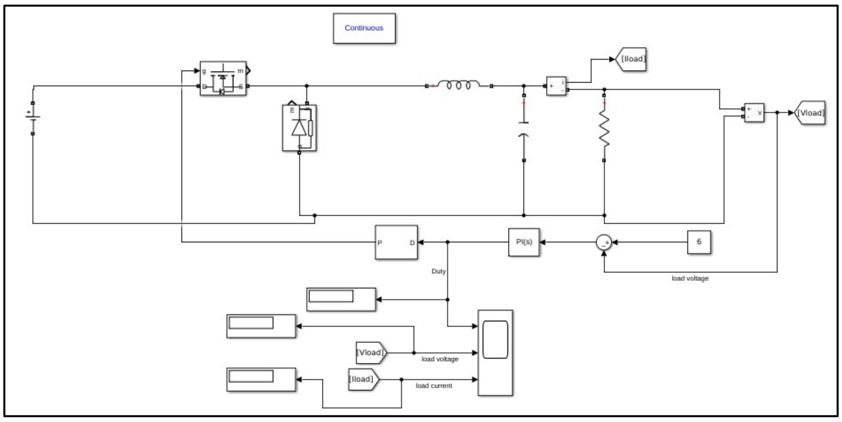

Fig.5. Buck converter schematic diagram with the PWM

The ideal buck converter output voltage is 5.831 V at a duty cycle of 0.2746 before turning on the PI controller. After tuning, the output voltage increases to 5.994 V with a duty cycle of 0.281 with the same load resistance. The PI values are 0.290 and 75.119, respectively, which means the duty cycle will quickly react to voltage changes and eliminate steady-state errors, thus ensuring the output voltage remains close to the desired 6 V. Figure 6 shows the variation of voltage output with capacitance. 100 µF results in the most stable voltage output compared to 30 µF and 68 µF. This shows that a higher capacitance minimizes voltage ripple and helps manage sudden load changes.

As expected, the current naturally decreased as resistance increased for all capacitance values, following Ohm's law. The fact that the output voltage remained constant, even with changes in current, highlights the importance of having larger capacitors to store energy. We also observed that the duty cycle dropped with rising resistance across all capacitance values, which makes sense given the lower current demand. The 100 µF capacitor's smoother and more consistent duty cycle curve indicates a better response and regulation.

Next, when simulating different values of input voltages, 24 V, 50 V, and 100 V with 1Ω load resistance, the voltage output stayed reliably close to 5.99 V. As the voltage input increased duty cycle value decreased to keep the output voltage steady at higher input levels. This result aligns with the buck converter's ideal equation. Throughout this process, the output current remained fairly stable, ensuring a consistent delivery to the load.

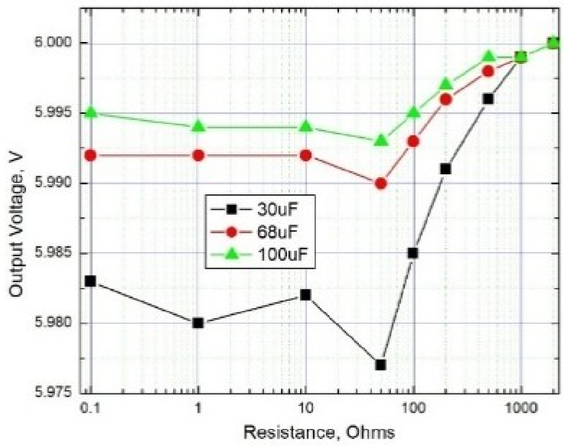

Fig. 6. Variation of the Output Voltage with Capacitance

3.2.2 Non-Ideal Case

Simulations were performed to analyse the circuit's behaviour in a non-ideal environment, considering parasitic resistances and diode forward voltage drops as shown in Fig. 7.

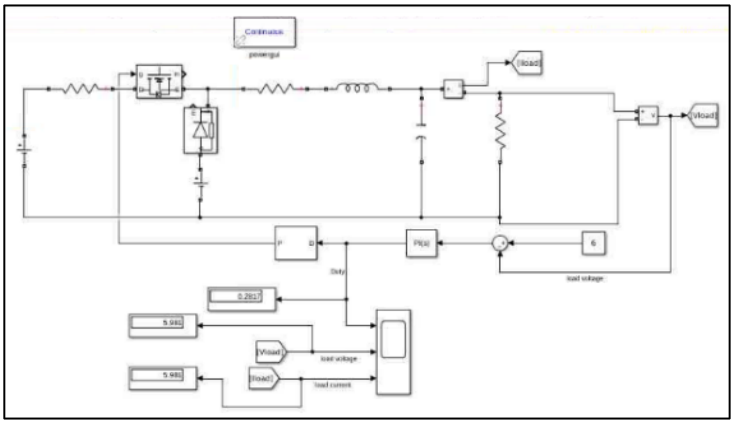

Fig. 7. Non-ideal Buck converter schematic diagram

Introducing a 50 mΩ series resistance before the inductor resulted in a slight dip in output voltage and current, particularly when the load resistance was low, thanks to those pesky I^2R losses. To make up for this, the converter ramped up the duty cycle. On a similar note, adding 50 mΩ resistance at the MOSFET also caused voltage and current drops under heavy loads, again due to increased losses. Plus, opting for a diode with a higher forward voltage of 0.7 V compared to 0.2 V further reduced output voltage and current during heavy loads, showcasing the efficiency perks of low V_f Components.

When accounting for diode losses, the ideal buck converter output voltage can be expressed in Eqn. 4.

$$V_{out} = D \times V_{in} - V_f \tag{4}$$

Thus, for V_f = 0.2 V, Vout was 5.8 V, and for V_f = 0.7 V, Vout dropped to 5.3 V.

The duty cycle had to increase to maintain the desired output voltage when diode losses were present. The modified duty cycle expression,

$$D = \frac{V_{out}+V_f}{V_{in}} \tag{5}$$

showed that for V_f= 0.2 V, D = 0.2583, and for V_f= 0.7 V, D = 0.2792. This clearly shows that a higher V_f means a higher duty cycle is needed to make up for the voltage lost during the off cycle. If all non-ideal factors are taken into account, the drop in output voltage and current becomes even more noticeable, and the duty cycle increases more dramatically.

The general buck converter equation, $V_{out} = D \times V_{in} - I \times R_{Total} - V_{Diode}$ effectively captures the behavior we observed, where R_{Total}includes the resistances of the MOSFET and the inductor. These simulations really underscore the vital need to consider component non-idealities in real-world converter designs to ensure they operate accurately and efficiently.

Table 2. The output values for a non-ideal simulation with load resistance 10Ω.

Non-ideal	Inductor		MOSFET		Diode		Combined			
	10mΩ	50mΩ	10mΩ	50mΩ	0.2V	0.7V	0.2V		0.7V	
							10mΩ	50mΩ	10mΩ	50mΩ
V_{out}, V	5.994	5.994	5.994	5.994	5.994	5.994	5.995	5.995	5.995	5.995
Current, A	0.5994	0.5994	0.5994	0.5994	0.5994	0.5994	0.5994	0.5994	0.5995	0.5995
Duty Cycle, D	0.2749	0.2759	0.2747	0.2748	0.2686	0.2534	0.2691	0.2702	0.2538	0.255

4. CONCLUSION

This paper provided a detailed look at the design process, covering key parameters like duty cycle, switching frequency, inductor and capacitor values, and the best choices for components. Since the buck converter was designed for general-purpose DC voltage regulation, it is suitable for both low-power and high-power applications. Additionally, a digital control system was effectively developed for the converter. The performance of this buck converter, with its digital control system, was examined and analysed through simulations using PSpice and MATLAB/Simulink. The research specifically chose Pulse Width Modulation (PWM) as the modulation technique, with its behaviour tuned by a Proportional-Integral (PI) controller to ensure precise output voltage. The simulations consistently showed that this control approach leads to a solid level of stability and impressive system performance for the digitally controlled buck converter.

REFERENCES

[1] 2021 18th International Multi-Conference on Systems, Signals & Devices (SSD), Monastir, Tunisia: IEEE, Mar. 2021, pp. 1419-1424. https://doi.org/10.1109/SSD52085.2021.9429371

[2] H. Sucu, T. Göktaş, and M. Arkan, "Design, Simulation and Application of Buck Converter with Digital PI Controller," Balk. J. Electr. Comput. Eng., vol. 9, no. 2, Art. no. 2, Apr. 2021. https://doi.org/10.17694/bajece.884290

[3] Gao, Linghao. (2025). Review of DC-DC Converters: Analysis and Applications of Buck and Boost Converters. Applied and Computational Engineering. 148. 14-18. https://doi.org/10.54254/2755-2721/2025.22314

[4] J. Linares-Flores et al., "Sliding Mode Control Based on Linear Extended State Observer for DC-to-DC Buck-Boost Power Converter System With Mismatched Disturbances," IEEE Trans. Ind. Appl., vol. 58, no. 1, pp. 940-950, Jan. 2022. https://doi.org/10.1109/TIA.2021.3130017

[5] Current waveform of each part. (1). Page 2. 2/6. Application Note. Capacitor Calculation for Buck converter IC. © 2012 ROHM Co., Ltd. No. 61AN104E Rev.004.https://fscdn.rohm.com/en/products/databook/applinote/ic/power/switching_regulator/capacitor_calculation_appli-e.pdf

[6] R. W. Erickson and D. Maksimović, Fundamentals of Power Electronics. Cham: Springer International Publishing, 2020. https://doi.org/10.1007/978-3-030-43881-4